

The Shishkhid ophiolite, northern Mongolia: A key to the reconstruction of a Neoproterozoic island-arc system in central Asia

A. Kuzmichev^{a,*}, A. Kröner^b, E. Hegner^c, Liu Dunyi^d, Wan Yusheng^d

^a *Geological Institute, Russian Academy of Sciences, Pyzhevsky 7, 119017 Moscow, Russia*

^b *Institut für Geowissenschaften, Universität Mainz, 55099 Mainz, Germany*

^c *Department für Geowissenschaften, Universität München, Theresienstraße 41, 80333 München, Germany*

^d *SHRIMP Isotope Laboratory, Chinese Academy of Geological Sciences, 26 Baiwanzhuang Road, Beijing 100037, China*

Received 19 January 2004; received in revised form 9 February 2005; accepted 7 April 2005

Abstract

The Shishkhid ophiolite is a well-preserved 13 km-thick mafic-ultramafic assemblage which comprises (from bottom to top): mantle tectonites (~6 km), layered and isotropic gabbro (~4.5 km), sheeted dykes (up to 0.5 km), a bimodal assemblage of basalt and rhyolite (up to 0.7 km), as well as andesitic pyroclastic rocks (~2 km). The volcanic rocks are overlain by a 3 km-thick sedimentary sequence showing progressive subsidence of the volcanic edifice after cessation of volcanism. The sedimentary unit is unconformably overlain by Ediacaran-Cambrian platform sediments. SHRIMP U-Pb dating of magmatic zircons from a rhyolite of the lower volcanic unit has yielded a concordant ²⁰⁶Pb/²³⁸U age of 800 ± 2.6 Ma which is interpreted to reflect the time of magma crystallisation.

Samples of the gabbro, the bimodal sequence, and andesitic unit show predominantly a calc-alkaline melt fractionation trend. The trace element patterns exhibit subduction-related characteristics such as high abundances of fluid-mobile elements and negative anomalies for Nb relative to La. The initial ϵ_{Nd} values of +6.9 to 0 indicate melting of variably depleted and heterogeneous upper mantle sources. These were probably produced by input of a component from subducted sediment. Two samples lacking large negative Nb-anomalies reveal distinct mantle sources not enriched with a slab-derived sedimentary component. We interpret them as melts from an upwelling heterogeneous asthenospheric source (initial ϵ_{Nd} of 3.2 to 6.9) in a rifting arc environment. The Nd-isotopes in a rhyolite sample from the bimodal mafic-felsic volcanic assemblage suggest an origin by melting of gabbroic lower crust, probably due to basaltic injections in the course of arc-rifting.

The tectonic setting for the Shishkhid ophiolite is inferred to be similar to that of the Izu-Bonin “back-arc knolls extensional zone”. The Shishkhid arc formed in the mid-Neoproterozoic and evolved through most of the late Neoproterozoic until it collided with a continental block at the end of the Neoproterozoic. This event is termed as the late Baikalian orogenic phase widely recognized in southern Siberia.

The Shishkhid ophiolite and related rocks have been traced for about 600 km, and similar units can be found in other Precambrian terrains of central Asia. Thus, the Shishkhid oceanic-arc system was a major tectonic feature of the Neoproterozoic

* Corresponding author.

E-mail address: kuzmich@ilran.ru (A. Kuzmichev).

Palaeo-Asian ocean. Its recognition suggests that the central Asian tectonic evolution encompassed the development of three generations of island arc systems replacing each other throughout the Neoproterozoic to early Palaeozoic.

© 2005 Elsevier B.V. All rights reserved.

Keywords: Baikalian orogeny; Central Asian foldbelt; Island arc rifting; Neoproterozoic; Supra-subduction zone ophiolite; Tuva-Mongolian Massif

1. Introduction

The Shishkhid ophiolite is a part of western Tuva-Mongolian Massif—one of several Precambrian terranes or microcontinents known in the Sayan-Baikalian region that fringe the southern part of the Siberian craton (Fig. 1). This area is a key region to reconstruct the Neoproterozoic–Palaeozoic tectonic history of a large part of the Central Asian foldbelt, as it preserves an almost complete record of tectonic events. The Shishkhid ophiolite is one of the largest mafic-

ultramafic bodies in central Asia and is shown on most regional maps. Being poorly studied it was usually included in a Vendian-Cambrian island-arc system of the Palaeo-Asian Ocean (Gibsher et al., 2001; Khain et al., 1995, 2002). However, we believe that this interpretation has oversimplified the tectonic history of Central Asian foldbelt. We relate the Shishkhid ophiolite to a distinct and extensive late Neoproterozoic island-arc system that collided with the ancient Tuva-Mongolian continental core at the end of the Neoproterozoic.

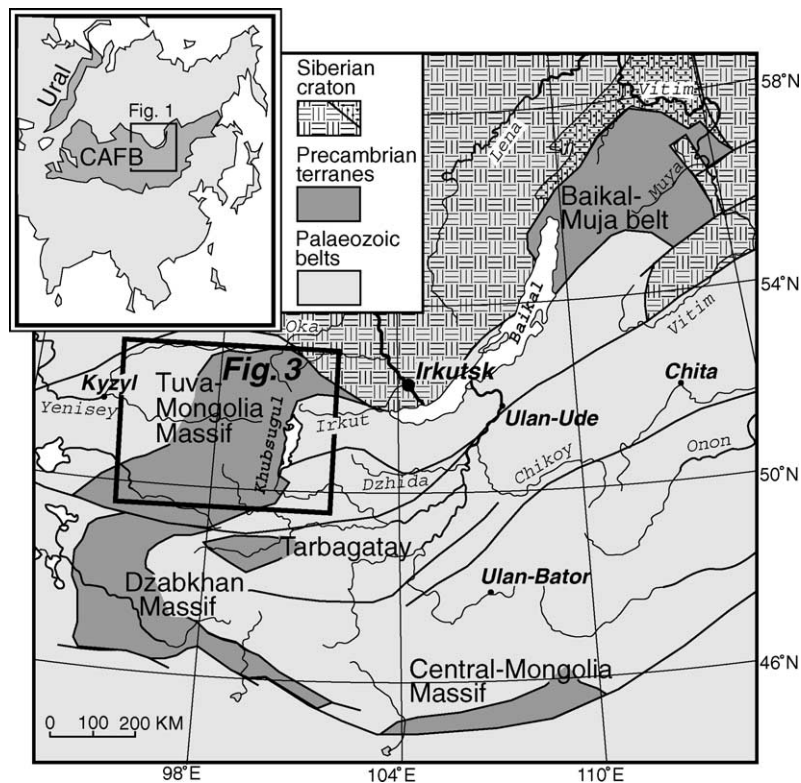


Fig. 1. Precambrian terranes in the Sayan-Baikalian region. Location of Central Asian fold belt (CAFB) is shown in the inset. An inset for Fig. 3 is indicated.



Fig. 2. Photograph of the Shishkhid ophiolite forming the ridge in the background. The lowland in front of the ridge is the source of the Ulyasutu River (Fig. 4. View to the south from point 249 (see Fig. 4).

The Shishkhid ophiolite (Fig. 2) is located in a remote area of northernmost Mongolia and its western tip extends into eastern Tuva. The ophiolite is exposed in an area over 70 km long and 15 km wide. Our study area lies to the north of the Shishkhid-Gol River and represents a unique region that was not affected by intense metamorphism and deformation, in contrast to areas farther north and south. Two sedimentary units with well established lithostratigraphy overlie the ophiolite complex and provide a minimum age for its formation.

This remote and mountainous part of northern Mongolia is difficult to access and thus poorly studied. An overview geologic map, at a scale of 1:500,000, is available for this region (A.B. Ilyin, et al., 1966, unpublished). More detailed mapping of the ultramafics of the lower part of the ophiolite was undertaken by Melaykhovetsky (1982). The large ultramafic body was studied in detail (Melaykhovetsky and Lesnov, 1976; Lesnov et al., 1977; Melaykhovetsky, 1982), but the overlying gabbro and volcanic units have not been investigated in detail to date. In 1988–1990, the senior author mapped the northern part of the ophiolite and adjacent areas, and this paper summarizes the results of the field observations and geochemical work.

The first purpose of this paper is to describe a distinct generation of late Neoproterozoic island arc systems

hitherto unknown in the Central Asian foldbelt. The second purpose is to attract the attention of petrologists to a ~13 km-thick complete section of the Shishkhid ophiolite. It represents uppermost mantle and rifted island-arc crust behind an oceanic arc, a setting that has not been suggested for known supra-subduction zone ophiolites.

2. Regional geological setting

The Shishkhid ophiolite lies in the Tuva-Mongolian Massif (Figs. 1 and 2). The latter is a traditional name, proposed by Ilyin (1971), though most of the “Massif” is built up of sedimentary and volcanic rocks which underwent low-grade metamorphism. The Tuva-Mongolian Massif differs from the surrounding Palaeozoic terrains by the presence of a Vendian to Cambrian platform cover, composed of carbonate sediments (Ilyin, 1971, 1982).

The main late Neoproterozoic rock complexes of the Tuva-Mongolian Massif are arranged in three distinct belts (Fig. 3). The eastern belt is the Sarkhoi volcanic belt (mostly ignimbrites) built on the ancient cratonic terrain, that was presumably part of the Siberian craton during most of the Neoproterozoic (Kuzmichev et al., 2001). The Sarkhoi belt represents a continental

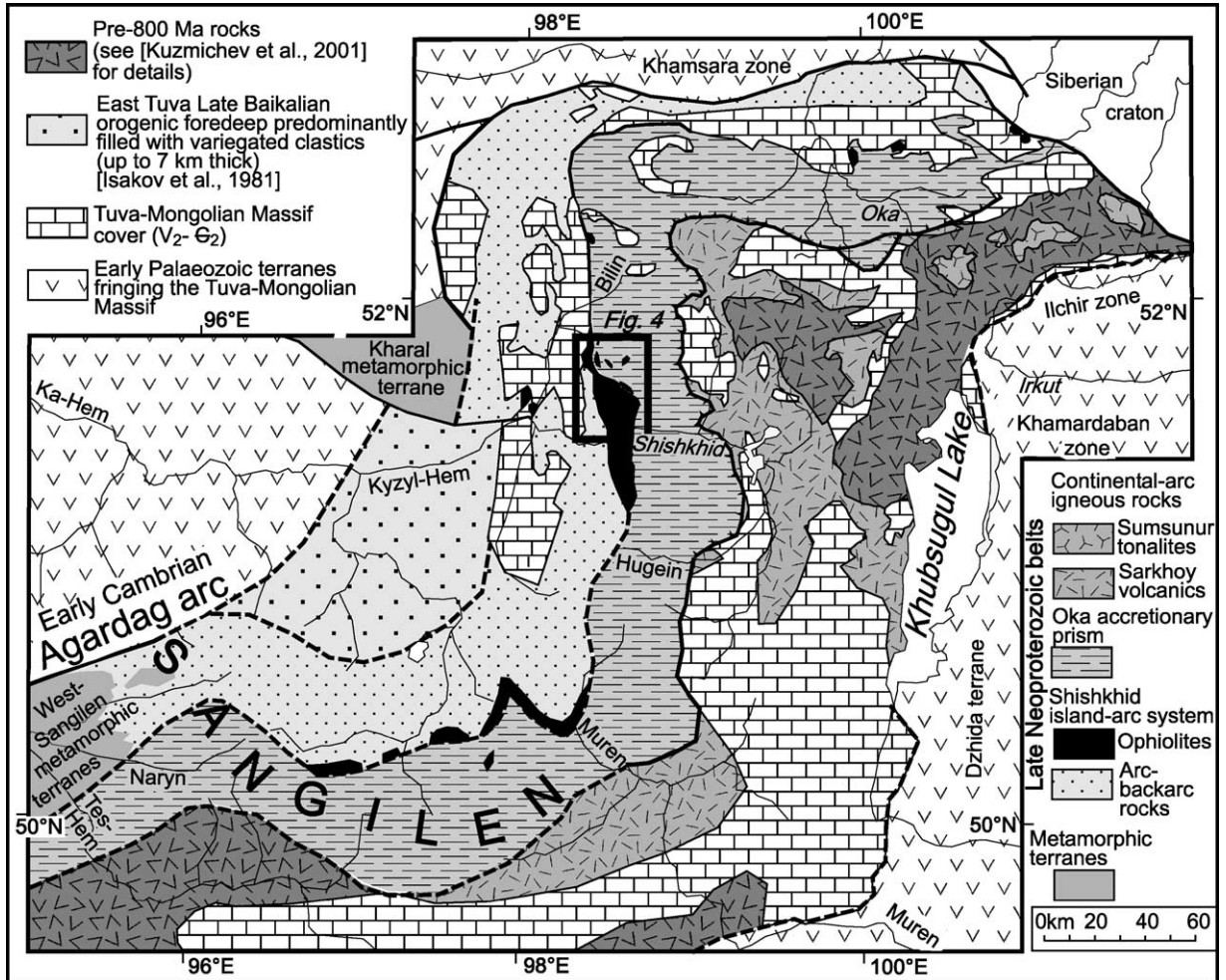


Fig. 3. Lithotectonic units of the Tuva-Mongolian Massif. The inset delineates the geological map shown in Fig. 4. Source: Isakov et al. (1981).

magmatic arc (Kuzmichev, 2004) and is fringed by the Oka belt, composed of shales, sandstones, and greenschists corresponding to a late Neoproterozoic accretionary prism (Sklyarov et al., 1996; Kuzmichev and Zhuravlev, 1999). This zone is bordered by a discontinuous ophiolite belt of which the Shishkhid ophiolite is the largest body. Ophiolites and related sedimentary and metasedimentary rocks constitute most of the outer zone of Tuva-Mongolian Massif, related in the Neoproterozoic to an oceanic arc.

The Shishkhid area is characterized by a nearly meridional structural trend and eastern structural vergence (Fig. 4). The ophiolite was thrust eastward onto the Oka belt and is tectonically underlain by a mélangé

zone comprising serpentinite lenses intercalated with shales of the Oka Formation. The mélangé zone is up to 5 km wide and 1 km thick. The Dogoilor-Gol syncline in the NW part of the area (Fig. 4) consists of an outlier of the Shishkhid ophiolite nappe and underlying mélangé.

In the west, the ophiolite is transgressively covered by greywacke and carbonate rocks of the Kharaberin Formation which, in turn, is overlain, unconformably, by Ediacaran to early Cambrian carbonate rocks of the Ailyg Formation (Kuzmichev, 1991). Since the entire region is overlain by the same platform carbonate deposits (Fig. 3), we postulate that the Shishkhid island-arc ophiolite was thrust upon the Oka prism

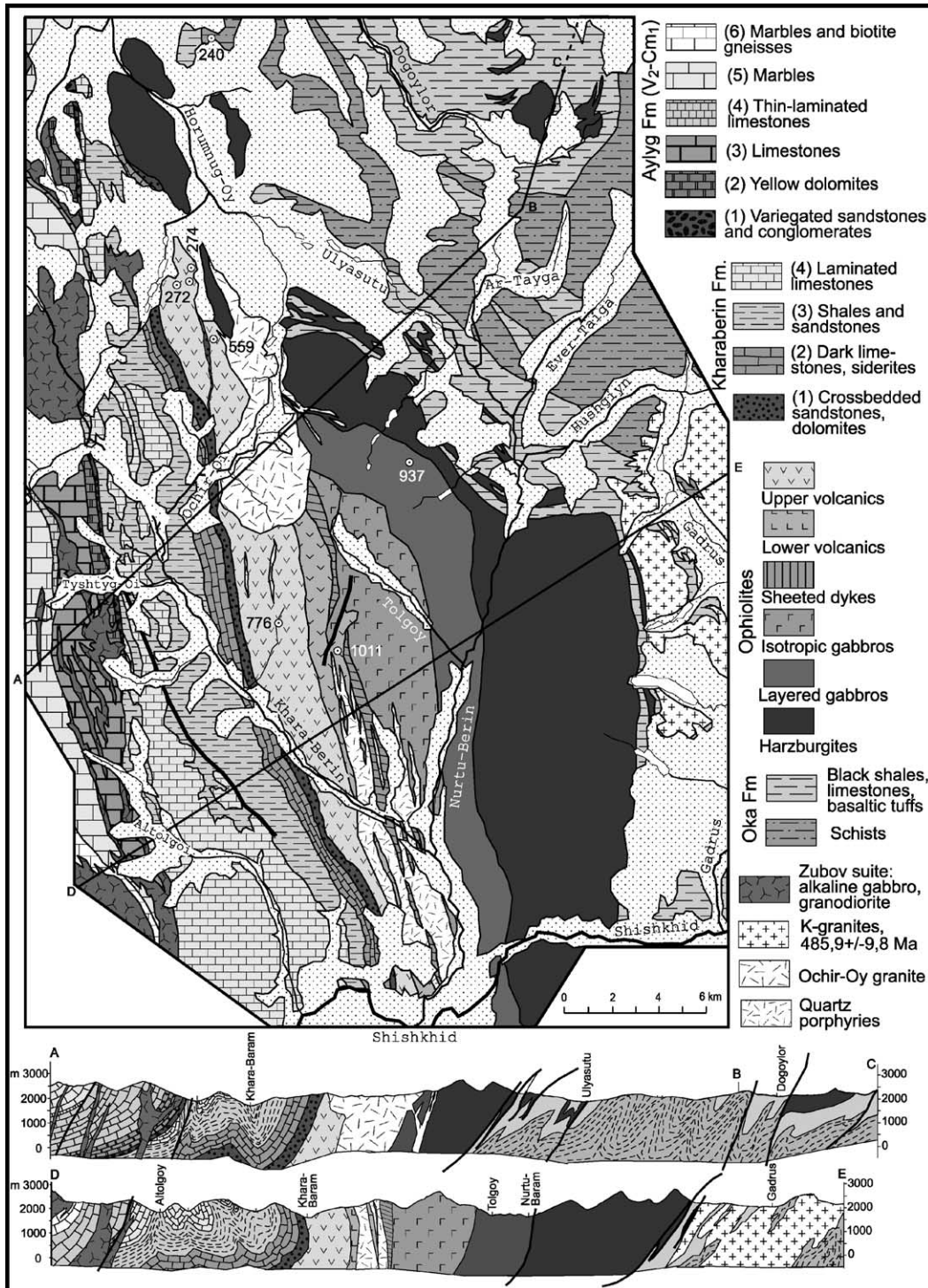


Fig. 4. Geological map of the Shishkhid ophiolite and associated rocks (simplified from Kuzmichev, 1990, unpublished).

prior to the end of the Neoproterozoic (Kuzmichev, 1991).

3. Lithological units of the Shishkhid ophiolite

The Shishkhid ophiolite includes from bottom to top: (1) residual ultramafic rocks, (2) layered (lower) and isotropic (upper) gabbros, (3) a sheeted dyke complex, and (4) lower and upper volcanic rocks (Fig. 5). The section represents the uppermost oceanic lithosphere, comprising depleted mantle tectonites of dunite–harzburgite composition (~6 km thick) and oceanic crust of basaltic composition (~7.5 km thick). It represents an almost complete crustal section with locally, as a result of thrusting, missing lower crustal components such as ultramafic cumulates and flaser-gabbros from near the Moho.

3.1. Residual ultramafic rocks

According to Melaykhovetsky (1982), the ultramafic sequence is dominated by harzburgite containing 10–15% enstatite and about 1% chromite. Dunites are also abundant, forming lenses and layers in the harzburgite. The cpx-bearing harzburgites are rare. Ultramafic rocks, except for local fresh occurrences, are completely or partly altered to antigorite serpentinite, rarely also to talc-carbonate. Graphitic harzburgite was also observed. Recrystallization and ductile deformation of primary minerals indicate that the rocks were deformed at high temperatures and may be referred to as mantle tectonites. The uppermost part of the ultramafic unit is a cumulate sequence (0–200 m thick) consisting of harzburgite, lherzolite, dunite, wehrlite and pyroxenite (Melaykhovetsky and Lesnov, 1976; Melaykhovetsky, 1982).

3.2. The lower gabbro unit

The lower boundary of the gabbros is a distinct thrust zone corresponding to the MOHO. The lower gabbro unit is chiefly composed of cumulates, though considerable areas comprise isotropic gabbro. As it is conventionally accepted, the upper boundary of the gabbros was defined as the zone where the ultramafic rocks and magmatic layering disappear (Figs. 4 and 5).

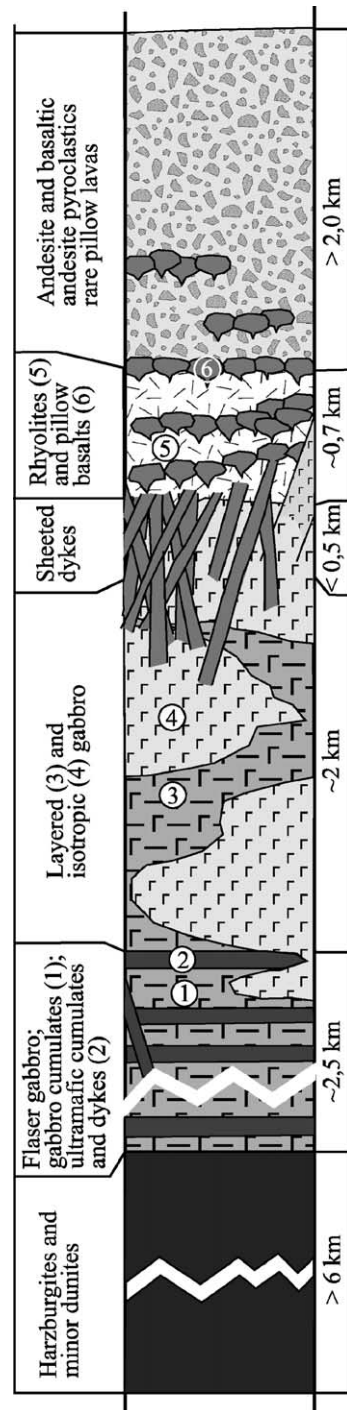


Fig. 5. General stratigraphy of the Shishkhid ophiolite. Circled numbers in the patterns refer to rock types given on the left hand side of the column.

The lower gabbro unit mainly comprises three rock types, namely cumulates of predominantly gabbroic composition, ultramafic cumulates, and isotropic gabbro. There are also minor cataclasites, mylonites, and small pods of microplagiogranite. Furthermore, the lower part of the unit contains some flaser gabbro which exhibits a ductile flow fabric.

Cumulate gabbros are represented by fine- and medium-grained, granoblastic, leucocratic to melanocratic rocks. They are locally strongly layered, and the transitions between the various rock types are usually gradational. Two rock groups can be distinguished, namely eucrite and ferruginous gabbro.

The eucritic gabbro is composed of clinopyroxene and anorthite, locally with minor olivine or orthopyroxene. Clinopyroxene is partially replaced by hornblende and/or actinolite, whereas anorthite is replaced by clinozoisite and prehnite. At places clinopyroxene is completely fresh, and the rocks are black and grey, lacking green colours. Some varieties contain orthopyroxene with clinopyroxene lamellae. Mineral proportions vary considerably, and the rock gradually changes from almost anorthositic to melanocratic gabbro with only 10–15% plagioclase.

Ferruginous gabbros exhibit deep-greenish-brown hornblende, abundant ilmenite-titanomagnetite, and apatite. Sphene either forms rims around ilmenite-titanomagnetite or completely replaces it. There is also a rare euhedral mineral, presumably kaersytitic hornblende, now replaced by chlorite, clinozoisite, and sphene.

The ultramafic cumulates consist of meta-dunites, wehrlites, and pyroxenites. They form layers of 0.2 m to several metres thickness. The olivine-bearing rocks are generally rusty-brown due to oxidation of magnetite and can be traced over considerable distances. Clinopyroxenites also occur as coarse-grained dykes. The primary mineral assemblage in the ultramafic rocks was clinopyroxene and olivine (up to monomineralic varieties), with small amounts of plagioclase (0–10%) and, in some cases, orthopyroxene. Olivine is now replaced by talc and serpentine; pyroxenes by hornblende, actinolite-tremolite, and chlorite.

Cataclasites and mylonites form numerous concordant zones on the eastern slope of the gabbro ridge at site 937 (Fig. 4). Cataclasites are micro-granular, sheared rocks which locally have preserved their original mineral composition or show secondary clino-

zoisite, amphibole, and prehnite. In the first case, fragmented crystals are scattered in a black matrix. Cataclasites gradually turn into mylonites which form zones varying in width from several millimetres to 100–120 m, resembling phyllites. The rocks are composed of fine grains of clinozoisite, chlorite, and actinolite in an opaque matrix. Locally, actinolite and zoisite form porphyroblasts. The main mylonite body (site 937, Fig. 4) contains unusual quartz veins up to 2 m wide, composed of deep black crystalline quartz.

Microplagiogranite is a fine-grained, grey rock composed of plagioclase, quartz, and amphibole. It contains numerous small zircons.

3.3. The upper gabbro unit

The upper portion of the gabbro unit is dominated by isotropic, eucritic gabbro. It also contains rocks showing subtle transitions to melanocratic or leucocratic gabbros. There is minor gabbro-diorite with andesine, as identified in thin section. Its relationship with the associated rocks is not clear. The isotropic gabbro, typical for this unit, is composed of Ca-plagioclase and clinopyroxene. The rocks are usually transected by a network of epidote veins and locally turn into gabbro breccia with a fine crystalline cement. Gradual transitions to fine-grained diabase-like varieties were also observed. There are also diabase dykes, frequently disrupted by en-echelon faults.

3.4. Sheeted dyke unit

It is difficult to recognize the sheeted dyke unit beneath the rock debris covering the slopes. However, it is well exposed along the first eastern tributary of the Kharaberin-Gol River. This section shows diabase dykes varying in width from several centimetres to one metre. One-sided chilled sheeted dykes and host gabbro screens were also observed. The sheeted dyke unit decreases in thickness to the north, where it is partly composed of non-parallel dykes.

3.5. Lower volcanic unit

It occurs south of the Ochir-Oj River, on the ridge between the Tolgoy-Gol and Kharaberin-Gol Rivers (Fig. 4). It is up to 700 m thick and comprises a bimodal basaltic-felsic assemblage. Basalt or basaltic andesite

are represented by pillows or massive lava flows. At places the top of massive lava flows turns into pillows. The pillows vary in size from small (5–10 cm) to large (up to 2 m in diameter). The space between the

pillows is filled with hyaloclastic breccia. The basalts contain occasional phenocrysts of clinopyroxene and abundant plagioclase microlites and laths. The latter form a doleritic framework in thick flows. The matrix

Table 1

Major-element (in wt.%, recalculated to 100% anhydrous basis) and trace element (in ppm) concentrations for Shishkhd ophiolite rocks

	Upper volcanics						Lower volcanics						
	531/1	555/3	772/1	772/2	774/1	781/2	1007/2	1007/3	1010/1	1011/4	1012/1	1013/1	1015/1
SiO ₂	60.98	54.19	55.13	57.13	57.49	55.06	73.39	78.33	48.64	49.35	51.18	49.93	48.94
TiO ₂	0.43	1.30	0.61	0.54	0.47	0.94	0.43	0.48	1.79	0.82	1.57	0.67	0.80
Al ₂ O ₃	18.40	17.86	20.64	20.05	18.12	17.19	14.72	12.17	15.24	14.84	15.46	16.06	14.98
Fe ₂ O ₃ *	6.86	10.62	8.88	7.67	6.38	10.98	3.37	1.44	13.75	11.69	12.76	9.94	12.28
MnO	0.15	0.18	0.14	0.14	0.14	0.18	0.14	0.04	0.20	0.18	0.18	0.16	0.18
MgO	3.43	5.94	3.79	3.57	5.74	5.99	2.40	0.64	7.45	12.38	6.36	10.14	12.10
CaO	4.76	6.57	7.96	8.01	5.95	7.17	0.80	1.36	10.16	7.99	9.07	11.41	8.82
Na ₂ O	4.75	2.63	2.51	2.07	5.45	1.93	3.41	4.12	2.44	1.45	3.16	1.46	1.13
K ₂ O	0.17	0.49	0.21	0.68	0.13	0.39	1.20	1.51	0.09	1.07	0.10	0.14	0.69
P ₂ O ₅	0.09	0.23	0.12	0.13	0.12	0.17	0.12	0.01	0.23	0.24	0.16	0.08	0.08
V	♥	♣ 297	♥	♥	♣ 147	♥	♥	♣ 29.7	♣ 343	♣ 247	♥	♥	♥
Cr		182			55.6			23.1	336	692			
Co		32.5			25.4			1.11	51.3	52.9			
Ni	50	52.8	48	49	60.9	32	11	15.0	187	391	94	217	295
Ga	40	18.5	19	27	11.6	19	23	11.4	20.7	15.8	27	32	28
Rb	<6	14.7	<6	9	0.90	11	19	24.7	1.01	16.7	<6	<6	8
Sr	107	444	146	210	167	571	142	82	372	132	190	128	112
Y	11	19.0	10	15	7.8	20	19	15.7	34.3	14.5	30	17	16
Zr	61	133	55	56	33	99	72	104	114	74	93	43	52
Nb		13.7		5	0.90			4.00	4.95	6.68	6		
Cs		0.32			0.027			0.27	0.10	0.16			
Ba		266			13.8		431	487	21.7	460	11	36	131
La		12.8	3.6	6.2	1.99	19	8.4	12.5	6.08	15.8	8.2	15	7.4
Ce		28.2	7.5	11	5.02	30	16	26.0	17.5	34.1	14	23	11
Pr		3.66			0.74			3.11	2.81	4.33			
Nd		16.2	12	9	3.51	20	13	11.8	13.7	17.2	15	16	9.8
Sm		3.65	1.7	2.2	1.06	3.8	2.6	2.35	4.09	3.25	3.9	3.5	3.5
Eu		0.99	0.66	0.67	0.43	1.2	0.54	0.55	1.47	1.05	1.5	1.2	0.72
Gd		3.58	2.2	2.1	1.39	3.3	2.7	2.54	5.37	3.26	4.8	3.7	2.5
Tb		0.54			0.23			0.41	0.89	0.49			
Dy		3.05			1.43			2.52	5.63	2.63			
Ho		0.66			0.30			0.57	1.19	0.53			
Er		1.68	1.2	2	0.89	2	2	1.82	3.44	1.51	3.7	1.9	1.7
Tm		0.25			0.13			0.28	0.49	0.20			
Yb		1.51	0.83	1.1	0.85	1.2	1.8	2.01	3.18	1.34	2.9	1.6	1.7
Lu		0.23			0.13			0.33	0.49	0.20			
Hf		3.38			1.04			3.01	3.00	1.99			
Ta		0.83			0.54			0.53	0.54	0.61			
Pb		4.74			0.53			4.14	2.10	1.52			
Th		1.84			0.256			1.77	0.365	1.86			
U		0.52			0.081			0.45	0.11	0.35			
Nb/Ta		16.51			1.67			7.55	9.17	10.95			
Zr/Hf		39.35			32.02			34.45	38.00	37.14			
(La/Yb) _N		6.05	3.10	4.03	1.67	11.31	3.33	4.44	1.37	8.42	2.02	6.70	3.11

Table 1 (Continued)

	Intrusion	Sheeted dikes					Single dike	Gabbro						
	721/1	668/3	668/4	668/4a	668/7	1005/1	668/2	922/1	922/3	922/4	1004/1	1004/2	943/1	
SiO ₂	71.58	55.78	51.19	53.17	51.83	58.04	53.20	50.31	50.23	50.13	55.54	51.05	46.01	
TiO ₂	0.72	0.55	0.86	0.80	0.66	0.44	0.76	0.15	0.09	0.18	0.23	2.30	0.90	
Al ₂ O ₃	14.98	20.01	15.15	14.99	15.23	16.40	18.90	22.86	21.34	22.00	19.25	13.48	16.68	
Fe ₂ O ₃ *	2.58	8.60	11.40	10.62	9.72	7.63	10.37	3.81	3.58	4.35	5.85	17.16	13.06	
MnO	0.07	0.15	0.18	0.17	0.16	0.16	0.16	0.13	0.13	0.13	0.15	0.21	0.18	
MgO	1.57	5.60	11.01	10.21	10.45	8.12	4.60	7.07	8.52	7.07	7.23	5.07	8.39	
CaO	1.72	5.43	7.79	7.63	9.88	4.40	8.29	14.90	15.66	14.89	9.17	9.10	14.36	
Na ₂ O	4.27	3.65	2.22	2.16	1.82	4.57	2.96	0.60	0.28	0.89	2.47	1.22	0.18	
K ₂ O	2.62	0.10	0.09	0.08	0.13	0.15	0.17	0.05	0.08	0.25	0.05	0.13	0.09	
P ₂ O ₅	0.07	0.12	0.12	0.16	0.10	0.08	0.58	0.11	0.08	0.10	0.06	0.28	0.14	
V	♥	♣	♥	♥	♣		♠	♠	♠	♠	♠	♠	♠	
Cr		227			299									
Co		125			735									
Ni		30.1			45.0									
Ga	12	87.2	276	208	246									
Rb	24	18.3	33	24	16.5									
Sr	81	0.64	<6	9	1.80		2.31	0.58	1.59	5.50	0.52	2.59	0.57	
Y	522	564	223	242	269		679	225	273	234	326	213	497	
Zr	22	12.5	16	36	14.0		18.1	4.50	2.49	5.47	5.52	63	18.1	
Nb	160	58.7	65	120	33.9		21.6	3.25	4.19	3.21	6.92	45.7	20.3	
Cs		1.20			1.06		1.23	0.09	0.13	0.07	0.36	3.13	1.52	
Ba		0.015			0.025		0.08	0.05	0.09	0.31	0.02	1.36	0.04	
La	1555	76.5			62.9		102	13.6	19.3	36.6	38.7	124	32.4	
Ce	25	2.85	4.3		1.87		7.14	0.47	0.55	0.47	1.41	9.06	5.09	
Pr	37	7.41	7.5		4.81		16.8	1.03	1.16	1.05	3.18	24.5	15.1	
Nd		1.11			0.75									
Sm	14	5.38	7.8		3.95		11.8	0.91	0.84	0.98	2.08	17.9	10.7	
Eu	2.8	1.44	2.6		1.25		3.06	0.36	0.28	0.45	0.62	6.40	2.92	
Gd	0.76	0.46	0.83		0.59		0.95	0.25	0.18	0.27	0.29	1.98	0.88	
Tb	1.0	1.66	2.4		1.74		3.05	0.50	0.41	0.71	0.80	7.95	2.83	
Dy		0.27			0.30									
Ho		1.76			2.08		2.84	0.65	0.40	0.84	0.87	9.51	2.79	
Er		0.41			0.50									
Tm	1.2	1.10	2.3		1.33		1.74	0.43	0.25	0.60	0.57	6.18	1.79	
Yb		0.17			0.21		0.23	0.07	0.03	0.10	0.07	0.89	0.25	
Lu	0.49	1.07	1.4		1.31		1.31	0.39	0.21	0.44	0.44	5.09	1.52	
Hf		0.17			0.20		0.20	0.06	0.03	0.07	0.06	0.72	0.26	
Ta		1.64			1.01		0.62	0.12	0.15	0.14	0.24	1.71	0.81	
Pb		0.20			0.20		0.06	0.01	0.01	0.01	0.03	0.12	0.05	
Th		1.26			1.60		1.26	0.25	0.37	0.29	0.73	1.27	0.68	
U		0.537			0.276		0.54	0.04	0.07	0.04	0.12	0.43	0.04	
Nb/Ta		0.13			0.073		0.14	<0.01	0.01	<0.01	0.03	0.11	0.01	
Zr/Hf		6.00			5.30		20.50	9.00	13.00	7.00	12.00	26.08	30.40	
(La/Yb) _N		35.79			33.56		34.84	27.08	27.93	22.93	28.83	26.73	25.06	
	36.44	1.90	2.19		1.02		3.89	0.86	1.87	0.76	2.29	1.27	2.39	

Explanations: major elements (except 1007/3 and 671/4) by XRF, United Institute of Geology, Geophysics and Mineralogy, Novosibirsk. Samples 1007/3 and 671/4 by conventional wet technique at Geological Institute, Moscow. Rare-earth and trace elements: ♣—ICP-MS (42 elements) at the Institute of the Mineralogy, Geochemistry and Crystal Chemistry of Rear Elements, Moscow; ♠—ICP-MS (37 elements) at the Institute of Earth Crust, Irkutsk; ♥—trace elements by XRF with powder, REE by single channel ICP at the Institute of Lithosphere, Moscow. The blank spaces denote no data.

is replaced by actinolite, chlorite, epidote, leucoxene, and pumpellyite.

Rhyolite and dacite occur as lava flows or breccias, with fine-grained and phyrlic texture. Zonation in plagioclase phenocrysts is common. Quartz phenocrysts are rounded and locally corroded with crystals up to 2 mm in size. Rare hornblende is generally replaced by secondary minerals.

Near site 1011 (Fig. 4), rhyolite fragments occur within hyaloclastite, filling the space between basaltic pillows. A rhyolite breccia has also been observed and contains occasional basaltic fragments sometimes preserved as pillows. These findings indicate that the mafic and felsic magmas of the bimodal volcanic suite were simultaneously erupted. The unit contains minor epiclastic breccia with mixed fragments, including andesite. Thus, intermediate rocks such as andesite, although subordinate in abundance, were erupted during emplacement of the predominantly bimodal mafic-felsic suite. Rhyolite decreases in abundance to the north and was not found north of the Ochir-Oy granite.

South of site 1011 numerous small quartz porphyry bodies intruded the sheeted dykes and uppermost gabbro. Locally they contain phenocrysts of blue quartz up to 5 mm in size. South of the Khara- and Nurtu-Berin-Gol River junction, the quartz porphyry turns into microgranite. Most of these felsic intrusions contain biotite and differ chemically from the rhyolites (Table 1, sample 721/1).

3.6. Upper volcanic unit

It is composed of andesite, basaltic andesite, and pyroclastic rocks. The latter show chaotically-oriented angular fragments 1–25 cm in size. There are epiclastic breccias composed of different fragments. The boundaries of the pyroclastic flows could not be identified. Pillow lavas and thin (0.3–0.5 m) amygdaloidal lava flows were observed in the lower part of the unit at sites 559 and 776.

The northern exposures of the upper volcanic unit (sites 272–274) reveal the least altered rocks such as porphyry with up to 50% by volume of greenish-brown hornblende and zoned andesine up to 3–4 mm in size. Southwards, the rocks are more altered and lack primary minerals. In some rock types a porphyric texture has been recognized, yet the unit appears to be predominantly aphyric.

The absence of compositional layering indicates that the upper volcanic unit consists largely of primary pyroclastic rocks that were not redeposited. They were mainly erupted in a submarine environment, though above the explosive compensation level, which is generally defined for andesitic magma at a water depth of 500 m or less (Stix, 1991; Cousinaeu, 1994).

4. Sediments overlying the volcanic units

The upper volcanic unit is overlain by sedimentary rocks defined as the Kharaberin Formation (Kuzmichev, 1991). The upper Khara-Berin River basin is recommended as the stratotype. This region is unique as it preserves a primary rock succession which cannot be recognized with confidence either to the N or S.

The lower boundary of the sequence is disrupted. The displacement is probably minor since the same horizon of the Kharaberin Formation occurs adjacent to the ophiolite's upper volcanic unit throughout the region. These sediments probably were deposited upon the volcanic basement. The formation may be divided into four units (Fig. 4).

The lowermost unit is about 300 m thick and composed of polymictic sandstones, siltstones, and brownish, sandy dolomites. Its lower part contains stromatolitic dolomite replaced by conglobreccia with tabular fragments. The orientation of stromatolites and cross-stratification in sandstones indicate top and bottom of the sequence. The unit contains layers of poorly sorted volcanic conglomerate, predominantly composed of felsite, and porphyry fragments, similar to the underlying rhyolites and comagmatic intrusions. Some conglomerates show high abundances of basaltic and andesitic fragments.

The overlying unit is about 600 m thick and consists of black and grey limestone, and dolostone. Its middle portion comprises siderite beds and unsorted greywacke.

The third unit is 1000–1200 m thick and mainly composed of rhythmically interbedded (5–20 cm) dark grey shales and sandstones. Locally the rocks exhibit slump folds and graded bedding. There are also unsorted non-layered greywacke replacing mudstone and rare-pebble conglomerate up to 50 m thick. Redeposited tephra beds were also found. They consist of

fragments of vesicular pumice, andesite, and locally felsite.

The fourth and uppermost unit is represented by bedded argillaceous grey limestone with an exposed thickness of 800–1000 m.

The Kharaberin Formation is a transgressive sedimentary sequence. The lower horizons include storm-broken layers deposited in a shallow-water environment near a volcanic edifice. The third unit, mainly composed of turbidites, is interpreted as a relatively deep basin deposit. The presence of tephra indicates synchronous volcanic activity with the deposition of Kharaberin sediments and a temporal shift of the volcanic front towards the west (in present coordinates) and away from the depositional area. The fourth unit is composed of carbonate ooze and was deposited far away from the source of volcanic or terrigenous clastic material.

5. Geochemistry of the ophiolite

5.1. Analytical methods

The chemical composition of the samples was analyzed at three laboratories in Russia. Major element concentrations were determined by XRF on glass tablets at the Institute of Mineralogy and Petrography (UIGGM) in Novosibirsk. The trace element concentrations for samples indicated by the card symbol “clubs” in Table 1 were determined at the Institute of Mineralogy, Geochemistry and Crystal Chemistry of Rare Elements (IMGRE) in Moscow. The analyses were carried out by ICP-MS after sample powder dissolution in teflon bombs. Data quality was monitored with the international rock standards BCR-1 and BCR-2 measured as unknowns. The results for the rock standards indicate that the data are accurate to within <8% (1 S.D.) for element concentrations >0.2 ppm. Samples indicated by “spades” were analyzed by ICP-MS at the Institute of the Earth’s Crust (Irkutsk), using a method outlined in Garbe-Schonberg (1993). Sample powders were decomposed using an open beaker method and, therefore, Zr and Hf concentrations may be too low due to incomplete dissolution of refractory phases. Trace element concentrations for samples indicated with “hearts” were determined by XRF on powder pellets at the Institute of the Lithosphere in Moscow.

For Sm-Nd isotopic work, the sample powders were spiked with a ^{150}Nd – ^{149}Sm tracer and dissolved in a mixture of HF–HClO₄. Separation of Sm and Nd and mass spectrometry were performed according to the procedures outlined in Hegner et al. (1995). The isotopic measurements were carried out on a MAT 261 mass spectrometer in a dynamic quadrupole mass collection mode. The $^{143}\text{Nd}/^{144}\text{Nd}$ ratios are normalized to $^{146}\text{Nd}/^{144}\text{Nd}=0.7219$. The external precision of the $^{143}\text{Nd}/^{144}\text{Nd}$ ratios is 1.2×10^{-5} as has been determined with our Ames Nd standard solution yielding 0.512142 ± 12 ($N=35$), corresponding to 0.511854 in La Jolla Nd standard. The ϵ_{Nd} values were calculated with the parameters of Jacobsen and Wasserburg (1980). Present-day values for the chondritic uniform reservoir (CHUR) are $^{147}\text{Sm}/^{144}\text{Nd}=0.1967$, $^{143}\text{Nd}/^{144}\text{Nd}=0.512638$.

5.2. Major element concentrations

The major element concentrations of samples are listed in Table 1 and are plotted against SiO₂ as melt fractionation index in Fig. 6. The majority of the Shishkhd samples have low Fe/Mg ratios for a given SiO₂ concentration, classifying them mostly as calc-alkaline in composition. K₂O concentrations, although probably not primary due to sample alteration, suggest low- to medium-K magma series (Table 1, Fig. 6, bottom). A gabbro sample (1004/2) and another from the lower volcanic unit show high Fe/Mg ratios and high TiO₂ concentrations, consistent with tholeiitic compositions. A large scatter in the data of the gabbroic samples can be explained by their cumulate mineralogy.

The rocks of the lower volcanic unit are bimodal mafic-felsic in composition, showing a distinct compositional gap between 61 and 71% SiO₂ (Fig. 6). The lack of a continuous liquid line of descent among these samples indicates that the rhyolites are not related to the mafic volcanic rocks by fractional crystallization. In the MgO versus SiO₂ diagram it can be seen that some of the mafic members of the bimodal unit have very primitive compositions.

The samples from the upper volcanic unit are andesitic in composition and chemically more evolved than the underlying mafic rocks. They show high Al concentrations as found in island arcs.

Samples from both volcanic units show considerable scatter for some elements. The large scatter among

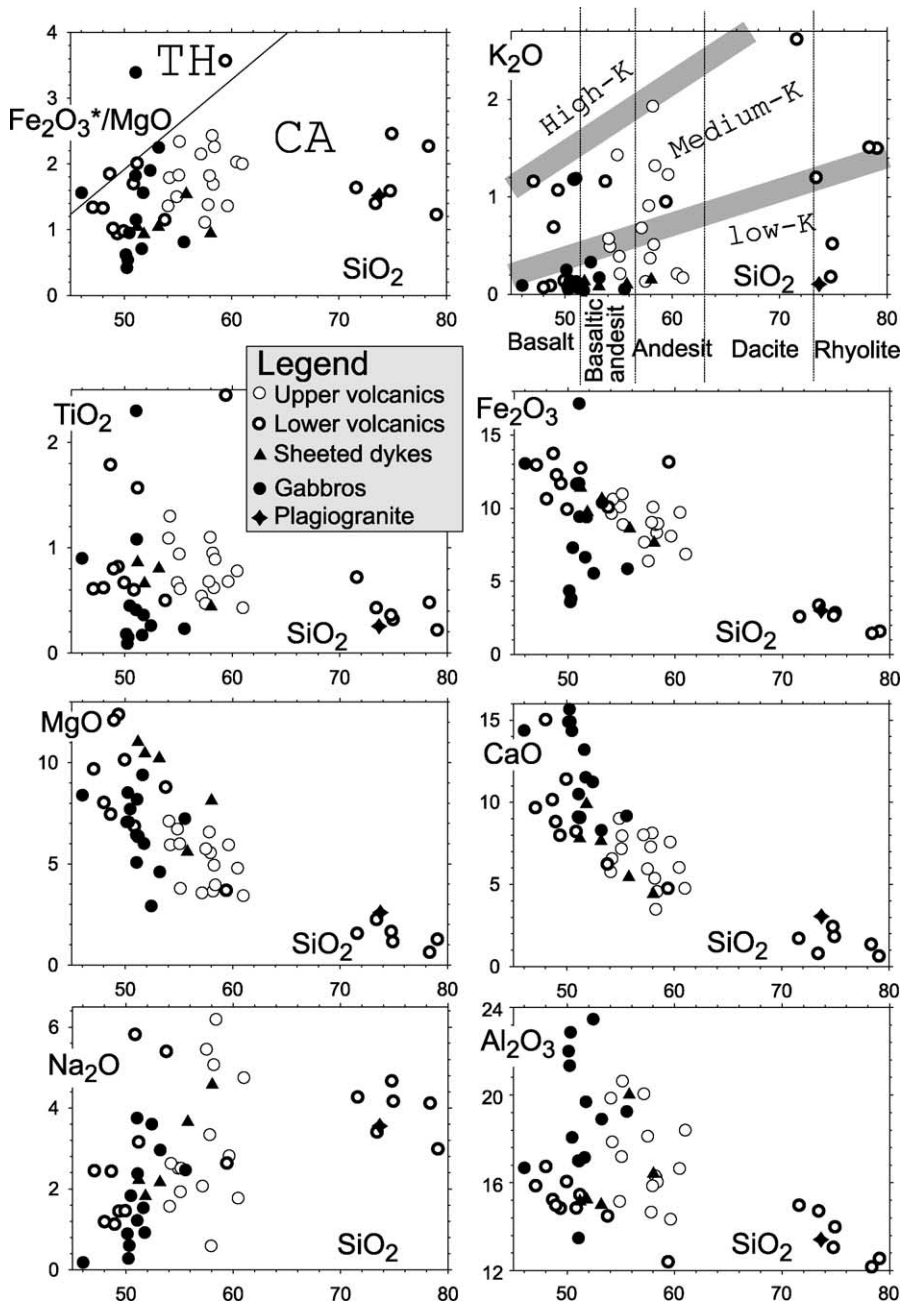


Fig. 6. Harker variation diagram for gabbros, dykes, and volcanic rocks of the Shishkhid ophiolite. TH—tholeiitic and CA—calc-alkaline compositions. Major element oxides in wt.% recalculated for an anhydrous composition. Note that the plotted data include unpublished analyses not listed in Table 1.

mobile elements such as K and Na can be attributed to sample alteration. However, the scatter among immobile elements such as Ti and Al is probably a primary feature of the samples. The large scatter of these elements at similar SiO₂ concentrations and degree of melt fractionation suggests that the samples probably belong to different melt batches.

5.3. Rare earth elements

The chondrite-normalized REE patterns for the gabbros show a large variation in REE concentrations due to the cumulate nature of some samples (Fig. 7, bottom). There are plagioclase cumulate varieties with positive Eu-anomalies and overall low total REE abundances, samples with LREE-enriched and HREE depleted patterns, as well as a single sample showing flat REE patterns with a negative Eu-anomaly. The sheeted dyke samples have flat to slightly enriched LREE patterns and positive as well as negative Eu-anomalies. Melt fractionation in the plagioclase stability field can explain the negative Eu-anomaly, whereas a positive anomaly indicates that the sample contains cumulate plagioclase. The HREE abundances are lower than in mid-ocean ridge basalts (MORB) with 10–20 times chondritic abundances. Two basalt samples from the bimodal volcanic unit exhibit very different REE patterns: whereas one sample shows a highly fractionated LREE/HREE pattern, the other sample displays an almost flat pattern with small depletion of La and Ce. A single sample of rhyolite shows a pattern enriched in the LREE and convex HREE. The latter reflects cpx- or hbl-control and a negative Eu-anomaly residual or fractionating plagioclase. The overlying andesites are moderately to strongly enriched in the LREE and show variable total REE abundances.

Thus almost each member of Shishkhid ophiolite assemblage shows diverse REE patterns. This may reflect different degrees of magma fractionation, different depth of magma generation as well as mantle source heterogeneity.

5.4. Normalized incompatible trace element patterns

The MORB-normalized trace element diagrams in Fig. 8 reveal a number of features underlining the calc-alkaline composition of the samples, as indicated by

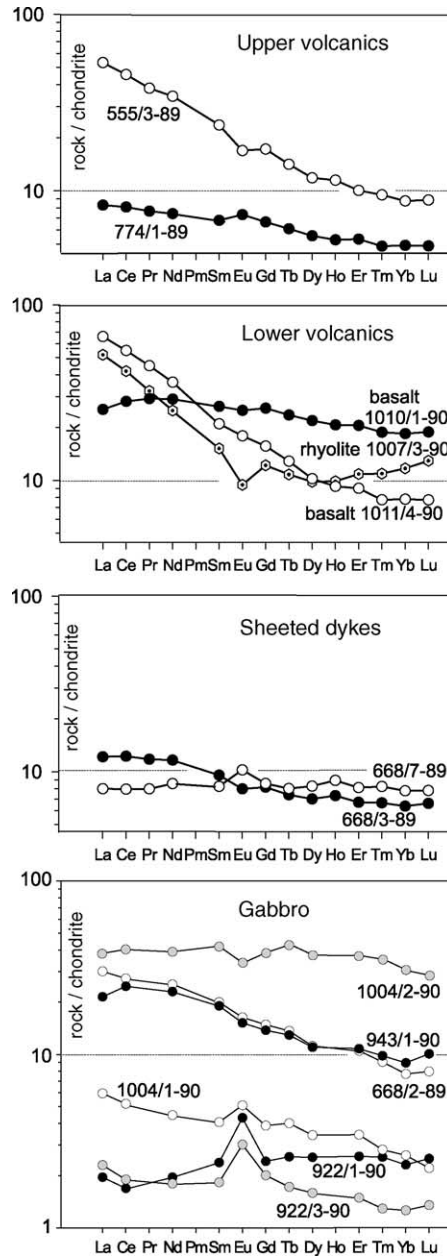
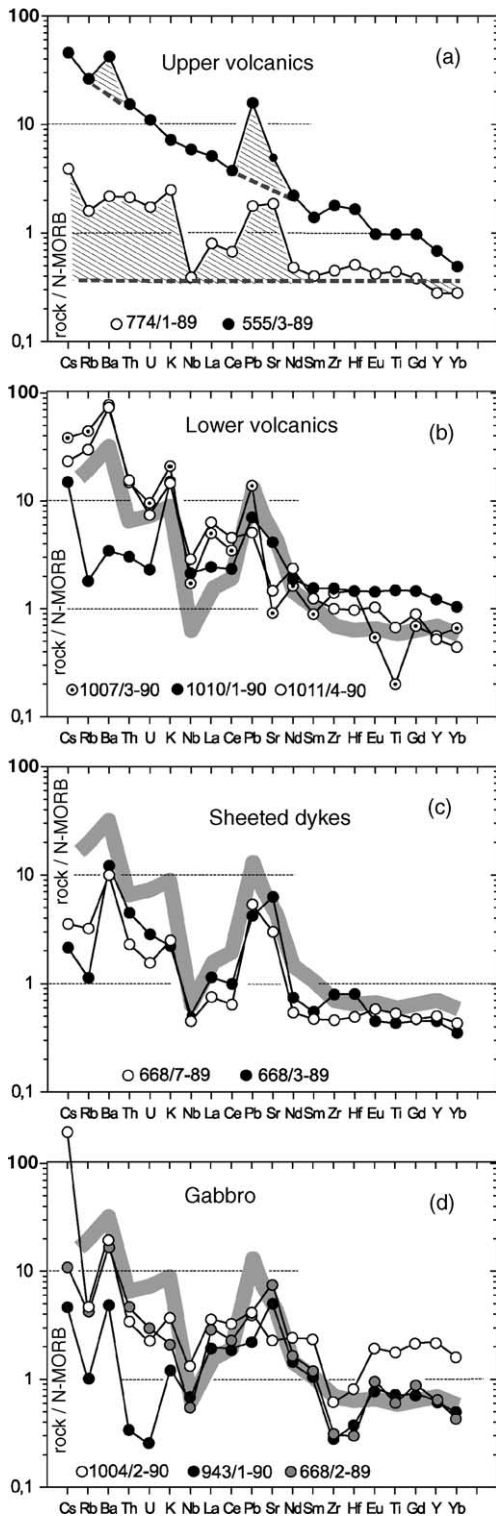


Fig. 7. Chondrite-normalized REE patterns for igneous rocks from the Shishkhid ophiolite. Normalizing values from Sun and McDonough (1989).

their low Fe/Mg ratio. High abundances of fluid-mobile elements such as Cs, in some cases K, Ba, Sr, and Pb as well as negative Nb-anomaly are typical of island-arcs (e.g. McCulloch and Gamble, 1991) and indicate



subduction-modified mantle sources. Systematic behaviour of the fluid-mobile elements in combination with the immobile REE and HFSE is good evidence that the overabundance of enrichment in fluid-mobile elements is a primary characteristic of most samples.

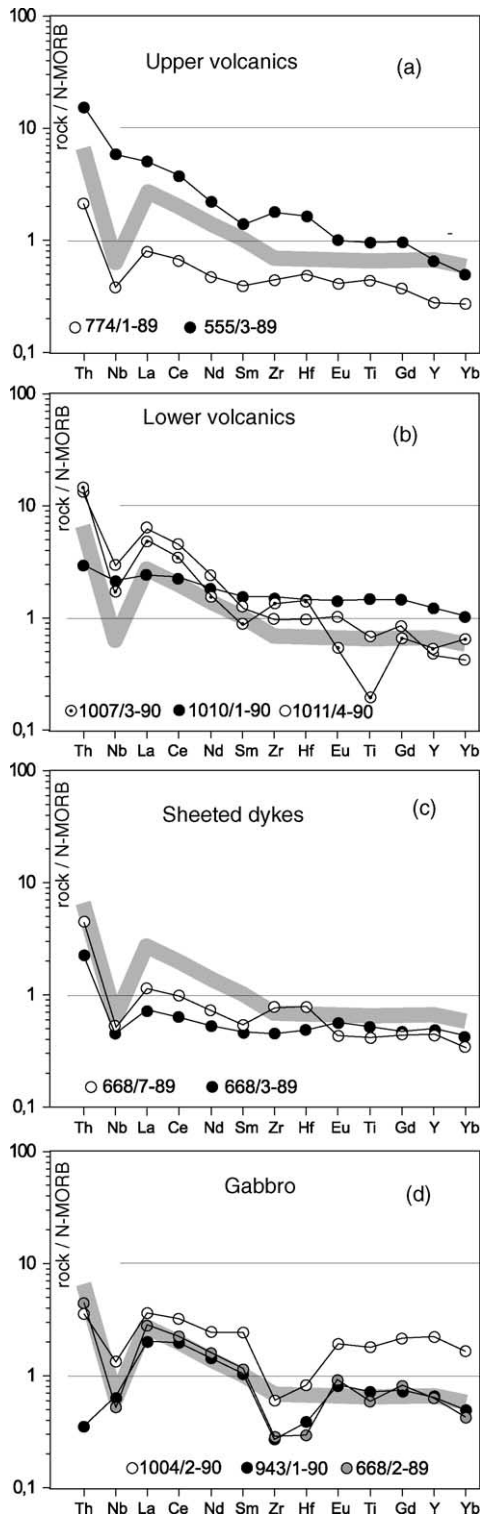
We are aware of the fact that the concentrations of mobile elements such the alkali and alkaline earths may to some extent be secondary due to sample alteration. In Fig. 9 trace element patterns, including only immobile elements, are shown. The salient features of these patterns are those of subduction-related rocks showing a distinct negative Nb-anomaly, high Th, and high La/Nb ratios for most samples. In two samples of the lower and upper volcanics a Nb-anomaly is virtually absent (Fig. 9). Obviously, these samples were derived from mantle sources that were less metasomatized by slab-derived fluids than those from which the other samples were produced.

5.5. Origin of the rhyolites

Felsic magmatic rocks can be produced in oceanic arcs due to (1) a shallow-depth fractional crystallization of basaltic or andesitic magma, (2) partial melting of an island-arc crustal source and (3) partial melting of a subducting young and hot oceanic slab (adakite) (Hochstaedter et al., 1990; Takagi et al., 1999; Tamura, 1995; Tamura and Tatsumi, 2002; Defant and Drummond, 1990; Drummond et al., 1996). The slab-derived melt model can be precluded here, since the Al_2O_3 , Y, and HREE concentrations in the Shishkhid rhyolites do not correspond to those in adakites.

The REE pattern for rhyolite sample 1007/3 (Fig. 7) has a U-shape and is complementary to that in hornblende, which largely concentrates the middle REE. This indicates hornblende as a residual or fractionating phase. A negative Eu-anomaly indicates fractionation and/or residual plagioclase. Thus, the Shishkhid rhyolites may have been produced by (1) fractional crystallization of andesitic magma, or (2) partial melting of a hornblende–plagioclase-bearing metagabbro.

Fig. 8. Normalized trace element patterns for igneous rocks from the Shishkhid ophiolite. Normalizing values from Sun and McDonough (1989). The grey band represents an average island-arc pattern (McCulloch and Gamble, 1991). Hatched patterns show the overabundance of elements interpreted as due to subduction-related overprinting of the mantle source.



The plagioclase–hornblende–phyric andesites, observed in northern Shishkhid outcrops, illustrate the possibility of separation of a felsic melt by filter pressing an intergranular liquid. Although the Shishkhid rhyolites could be produced by fractional crystallization combined with filter-pressing, this does not explain the most remarkable property of the lower volcanics, namely their distinctly bimodal composition. The bimodal composition favours the second option namely shallow-level partial melting of amphibolite. Underplating of hot high-Mg basaltic melts could have acted as a heat source. Thus, we propose that the Shishkhid bimodal sequence was produced in a similar fashion as bimodal sequences in continental rifts with massive crustal underplating of mantle-derived melts and melting of lower crust. This conclusion is further supported by the Nd isotopic systematics presented below.

5.6. Nd isotopic compositions

Ten samples representing all crustal units of Shishkhid ophiolite show initial ϵ_{Nd} ranging from +6.9 to 0.0. Most of the samples show a more restricted range of ca. +3 to +6.9 (Table 2, Fig. 10). Although all volcanic rocks exhibit incompatible element enriched patterns, the positive ϵ_{Nd} values reveal sources that evolved with a depletion in incompatible elements. Thus, their enrichment in incompatible elements must be due to overprinting of their mantle sources shortly before melting by slab-derived fluids and melts. Rhyolite sample 1007/3 from the bimodal suite and gabbro sample 668/2 have identical initial ϵ_{Nd} values of 0. This agreement supports an origin of the rhyolite from the gabbro by partial melting as discussed above. The Sm–Nd isotopic systematics of partial melting of gabbro are depicted and discussed in Fig. 11.

Each of the igneous units of the ophiolite contains a number of samples with highly positive ϵ_{Nd} values (Fig. 10), indicating that a highly depleted mantle source was the predominant source for the ophiolite sequence. In this context an explanation for the low ϵ_{Nd} values in some samples is required. The isotopic

Fig. 9. Normalized immobile-trace element patterns for igneous rocks from the Shishkhid ophiolite. Note that the very low concentrations of Zr and Hf in gabbros (bottom diagram) are probably due to incomplete dissolution of sample powder (see Section 5.1).

Table 2
Sm–Nd isotopic data for igneous rocks from the Shishkhid ophiolite

Sample	Rock type	Age (Ma)	Nd (ppm)	Sm (ppm)	$^{147}\text{Sm}/^{144}\text{Nd}$	$^{143}\text{Nd}/^{144}\text{Nd}$	$\epsilon_{\text{Nd}(t)}$
943-1	Gabbro	800	10.59	2.55	0.1458	0.512547	3.4
1004-2	Gabbro	800	18.30	5.82	0.1921	0.512951	6.6
668-2	Gabbro	800	11.03	2.77	0.1519	0.512404	0.0
668-3	Sheeted dike	800	6.05	1.66	0.1656	0.512787	6.1
668-7	Sheeted dike	800	4.22	1.35	0.1939	0.512883	5.1
1007-3	Rhyolite	800	12.64	2.46	0.1175	0.512225	0.0
1010-1	Basalt	800	14.96	4.52	0.1826	0.512919	6.9
1011-4	Basalt	800	21.15	4.02	0.1151	0.512481	5.3
555-3	Basaltic-andesite	800	15.73	3.48	0.1337	0.512474	3.2
774-1	Andesite	800	3.88	1.16	0.1813	0.512844	5.6

$^{143}\text{Nd}/^{144}\text{Nd}$ normalized to $^{146}\text{Nd}/^{144}\text{Nd} = 0.7219$. Within-run precision for $^{143}\text{Nd}/^{144}\text{Nd} < 1.2 \times 10^{-5}$. External precision for $^{143}\text{Nd}/^{144}\text{Nd}$ ca. 1.2×10^{-5} . Error for $^{147}\text{Sm}/^{144}\text{Nd} \sim 0.2\%$ (2σ). Ames Nd standard yielded: $^{143}\text{Nd}/^{144}\text{Nd} = 0.512142 \pm 12$ (2σ , $N = 35$).

variability may either reflect the isotopic heterogeneity of the upper mantle sources or may be due to overprinting of a highly depleted mantle with melts from subducted sediment with low ϵ_{Nd} values.

The magnitude of overprinting of the mantle wedge by a slab-derived component can be evaluated with the help of the Th/Nb ratio plotted versus initial ϵ_{Nd} values in Fig. 12. We consider basalt sample 1010/1 with an ϵ_{Nd} value of 6.9 and low Th/Nb ratio as being derived from the depleted mantle that was not metasomatized by fluid or melt. The samples with the lowest ϵ_{Nd} values (gabbro 668/2 and cognate rhyolite

1007/3) show the highest Th/Nb ratios of all samples. This is consistent with the suggestion that low ϵ_{Nd} is due to a significant amount of material from sediment in the mantle source. Overlapping of the data points of the rhyolite and its parental gabbro indicates that the Th/Nb ratio was not significantly fractionated during partial melting of the gabbro at crustal levels. The data of other samples do not plot on a mixing line between

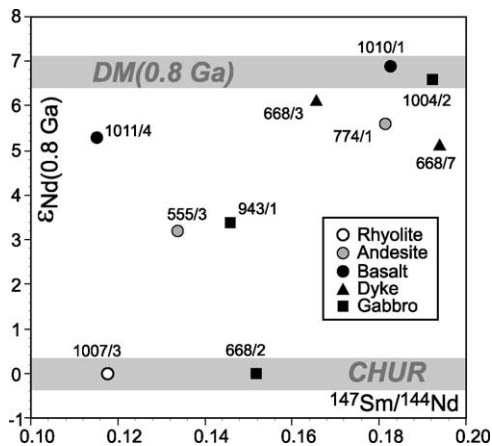


Fig. 10. Initial ϵ_{Nd} values versus $^{147}\text{Sm}/^{144}\text{Nd}$ ratios for igneous rocks from the Shishkhid ophiolite. Low $^{147}\text{Sm}/^{144}\text{Nd}$ ratios (< 0.1967) indicate flat to enriched LREE patterns in the samples. ϵ_{Nd} values, varying from 0 to +6.9, indicate isotopic evolution of their mantle sources with apparently unfractionated to highly depleted LREE patterns (see Section 5.6 for discussion).

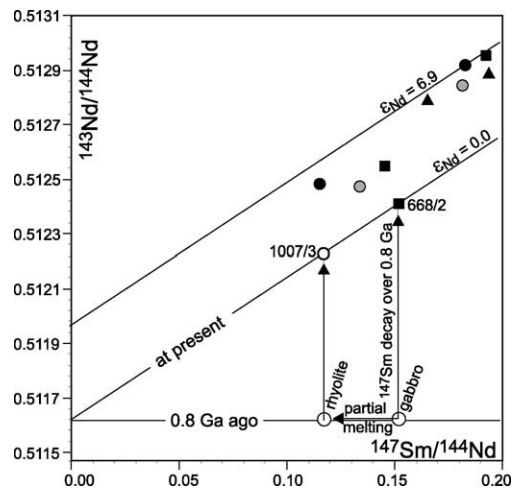


Fig. 11. Sm–Nd isotopic diagram showing evolutionary relationship between gabbro 668/2 and rhyolite 1007/3. As both samples have the same initial Nd isotopic composition, we suggest that the rhyolite is a partial melt of the gabbro. The consequences of partial melting of the gabbro are outlined: the rhyolitic partial melt would have a higher abundance of LREE and a lower $^{147}\text{Sm}/^{144}\text{Nd}$ ratio than the parental gabbro. Decay of ^{147}Sm over 0.8 Ga is shown by vertical arrows pointing to the measured Sm and Nd isotopic composition in the samples. Symbols as in Fig. 10.

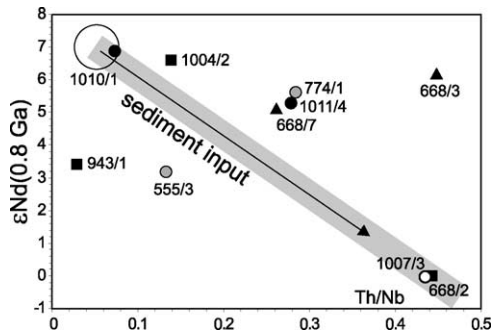


Fig. 12. ϵ_{Nd} values vs. Th/Nb ratios for selected samples of the Shikhid ophiolite (symbols as in Fig. 10). The Th/Nb ratio is interpreted as a tracer of subduction-related overprinting of the mantle source. Th is less mobile in hydrothermal fluids than LILE and reflects mantle metasomatism. Nb is immobile in fluids and has low concentrations in sediment-derived melts and, therefore, the Th/Nb ratio in such melts would be high. The low Th/Nb ratios in samples 1010/1 and 555/3 suggest little or no input of a sediment-component into their mantle source. Thus, the variation in Nd isotopic compositions in these samples may be primarily due to mantle heterogeneities unrelated to plate subduction. Other samples showing elevated Th/Nb ratios may have inherited a subduction-related component. The grey band is a mixing line between two end members: N-MORB (large circle) which is similar to sample 1010/1 and gabbro 668/2 showing the strongest evidence for being derived from an overprinted source.

the basalt 1010/1 and gabbro 668/2 endmember compositions. The position of data points to the right of the mixing line can be explained by source heterogeneity and/or by Th input from sediments. Two samples show low Th/Nb ratios indicating negligible overprinting of the mantle source by a slab-derived component. These are basalt 1010/1 and basaltic andesite 555/3. We interpret their ϵ_{Nd} values of +6.9 and +3.2 as evidence for heterogeneous mantle sources unrelated to those from which the other samples were derived. Sample 943/1 (Fig. 12) was not included in this group as it shows high Nd/Nb ratio that may reflect sediment input.

We conclude that probably two different mantle reservoirs were involved in the genesis of the Shikhid igneous rock assemblage: the main reservoir was the depleted sub-arc mantle, metasomatized by subduction-related fluids and slab-derived melts of sediment. The second mantle source was possibly the upwelling asthenosphere in a back-arc (?) environment. This mantle source may account in particular for the samples showing poorly developed subduction-related signatures, e.g. small negative Nb-anomalies.

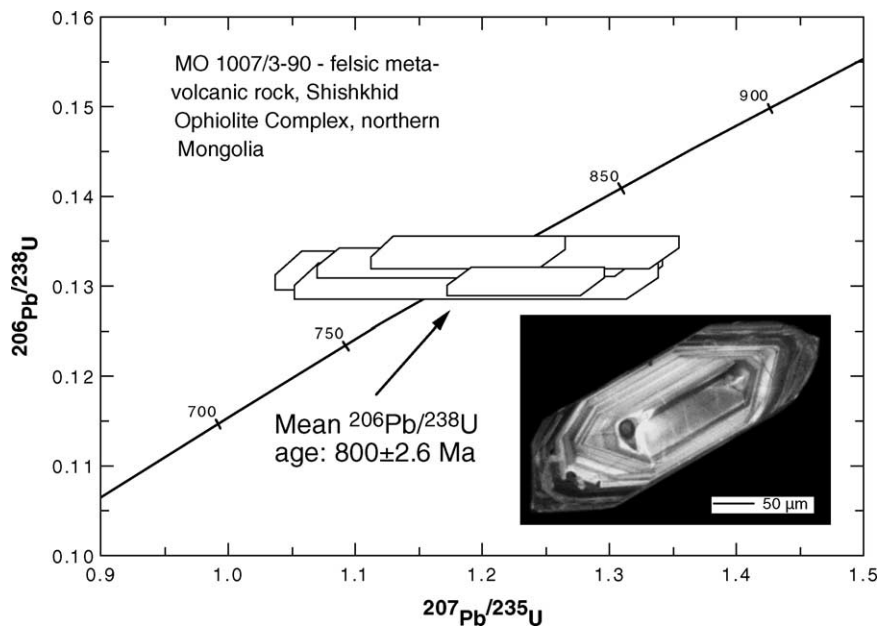


Fig. 13. Concordia diagram showing SHRIMP analyses of single zircons from rhyolite sample MO 1007-3-90, Shikhid Complex, northern Mongolia. Data boxes for each analysis are defined by standard errors in $^{207}Pb/^{235}U$, $^{206}Pb/^{238}U$ and $^{207}Pb/^{206}Pb$. Inset shows cathodoluminescence photograph of zircon grain with analyzed spot.

6. SHRIMP U–Pb zircon dating of rhyolite

Small clear, euhedral zircons some 40–100 μm in length from a rhyolite of the lower volcanic unit (sample 1007/3–90) were handpicked and mounted in epoxy resin together with chips of the Perth Consortium zircon standard CZ3. Cathodoluminescence (CL) imaging was performed on a JEOL JXA-8900RL superprobe at the University of Mainz with operating conditions at 15 kV accelerating voltage and 12 nA beam current. CL-images of zircons show oscillatory zoning typical of magmatic growth, and most grains have low-U cores with high-U rims (Fig. 13, inset). Internal structures show high-U (dark) and low-U (bright) domains (Vavra, 1990). Some subtleness in zonation is often visible and is particularly useful for recognizing inherited cores, overgrowth patterns, and phenomena associated with metamictization and/or recrystallization (e.g., Vavra, 1990; Hanchar and Miller, 1993; Vavra et al., 1996; Pidgeon et al., 2000).

Isotopic analyses were performed on the SHRIMP II ion microprobe at the Chinese Academy of Geological Sciences in Beijing whose technical specifications are identical to those of SHRIMP II at Perth, Australia (Kennedy and De Laeter, 1994). Analytical procedures are described in Compston et al. (1992) and Nelson (1997). The reduced $^{206}\text{Pb}/^{238}\text{U}$ ratios were normalized to the value of 0.09432, which is equivalent to an age of 564 Ma for the CZ3 standard. The error in the ratio Pb^*/U during analysis of all standard zircons during this study was 1.01%. Primary beam intensity was about 3.4 nA, and a Kohler aperture of 120 μm diameter was used, giving a slightly elliptical spot size of about 25 μm . Peak resolution was about 5000, enabling clear separation of the ^{208}Pb -peak from the nearby HfO_2 -peak. Sensitivity was about 23 cps/ppm/nA Pb. Analyses of samples and standards were alternated to allow assessment of Pb^*/U^+ discrimination. Raw data reduction followed the method described by Nelson (1997). Common-Pb corrections have been applied using the ^{204}Pb -correction method, assuming that common lead is surface-related (Kinny, 1986) and has the isotopic composition of Broken Hill lead. The analytical data are presented in Table 3. Errors on individual analyses are given at the 1σ level and are based on counting statistics and include the uncertainty in the standard U/Pb age (Nelson, 1997). Errors for pooled analyses are at 2σ or 95% confidence interval.

Table 3
SHRIMP II analytical data for spot analyses of single zircons from rhyolite sample 1007/3–90, Shishkhid ophiolite complex, northern Mongolia^a

Grain no.	U (ppm)	Th (ppm)	$^{206}\text{Pb}/^{204}\text{Pb}$	$^{208}\text{Pb}/^{206}\text{Pb}$	$^{207}\text{Pb}/^{206}\text{Pb}$	$^{206}\text{Pb}/^{238}\text{U}$	$^{207}\text{Pb}/^{235}\text{U}$	$^{206}/^{238}$ age $\pm 1\sigma$	$^{207}/^{235}$ age $\pm 1\sigma$	$^{207}/^{206}$ age $\pm 1\sigma$
Grain 1.1	86	56	2099	0.2494 \pm 84	0.0686 \pm 33	0.1304 \pm 15	1.233 \pm 62	790 \pm 9	816 \pm 28	887 \pm 98
Grain 2.1	69	54	1105	0.2600 \pm 113	0.0631 \pm 44	0.1323 \pm 16	1.151 \pm 84	801 \pm 9	778 \pm 39	711 \pm 149
Grain 3.1	36	16	844	0.1910 \pm 192	0.0663 \pm 79	0.1303 \pm 20	1.191 \pm 144	789 \pm 11	797 \pm 67	817 \pm 247
Grain 4.1	61	38	1751	0.2389 \pm 103	0.0645 \pm 40	0.1335 \pm 17	1.187 \pm 77	808 \pm 10	795 \pm 35	757 \pm 131
Grain 5.1	52	33	1522	0.2306 \pm 117	0.0687 \pm 46	0.1336 \pm 18	1.265 \pm 89	808 \pm 10	830 \pm 40	888 \pm 140
Grain 6.1	37	17	1008	0.2253 \pm 205	0.0654 \pm 83	0.1315 \pm 21	1.187 \pm 154	797 \pm 12	794 \pm 71	788 \pm 269
Grain 7.1	45	27	998	0.2340 \pm 142	0.0665 \pm 57	0.1327 \pm 18	1.217 \pm 107	803 \pm 109	808 \pm 49	823 \pm 179

^a 1.1 is spot 1 on grain 1, 2.1 is spot 1 on grain 2, etc.

Seven single zircons were analyzed and produced concordant data (Table 3, Fig. 13) with a mean $^{206}\text{Pb}/^{238}\text{U}$ age of 800 ± 2.6 Ma. We interpret this to reflect the time of crystallization of the felsic lava and it constitutes an upper age limit for extrusion of the ophiolite crustal rocks. Hence, the Shishkhid arc formed in the mid-Neoproterozoic.

7. Tectonic setting of the Shishkhid ophiolite

7.1. Diagnostic features

The diagnostic features to define the tectonic setting of the Shishkhid ophiolite include (1) geochemical characteristics of a supra-subduction zone for most igneous rocks; (2) bimodal rift-related composition of the lower volcanic unit; (3) an extensional tectonic regime manifested by the sheeted dykes; (4) heterogeneous mantle sources, including domains slightly or not influenced by subduction-related components. The setting that conforms to the above criteria is a rifted oceanic island arc system. Well-studied Cenozoic arcs reveal two types of geodynamic regimes that can explain that of the Shishkhid. These are (1) an early stage of intra-oceanic subduction, and (2) intra-arc to back-arc rifting. Volcanic rocks in other supra-subduction settings do not resemble those of the Shishkhid ophiolite sequence.

7.2. Origin of the supra-subduction zone (SSZ) ophiolite by initiation of intra-oceanic plate subduction

An intra-oceanic plate subduction setting is accepted as possible tectonic environment for the Shishkhid ophiolite because the majority of studied SSZ ophiolites are interpreted to have originated in this environment (Shervais, 2001, and references therein). An early phase of oceanic subduction is a specific regime which currently does not seem to operate anywhere on Earth. The best example of oceanic crust that formed in such a fashion is the Eocene Izu-Bonin-Mariana (IBM) forearc igneous basement (Leitch, 1984; Stern and Bloomer, 1992; Pearce et al., 1992; Arculus et al., 1992; Bloomer et al., 1995).

The Shishkhid ophiolite and the overlying Kharaberin Fm. share an evolution similar to that

observed in the borehole sections from the IBM forearc. The volcanic rocks in the section's lower part are mainly composed of deep-water pillow basalts, whereas the uppermost volcanic rocks comprise pyroclastic flows and lavas, erupted in shallow water or, locally, in a subaerial environment. The sedimentary sequence overlying the magmatic basement has accumulated during subsidence. Its lower part comprises volcanic breccias and turbidites, whereas the upper part is made up of marly and pelitic ooze (Lagabriele et al., 1992). However, such a succession is not specific for forearcs but can be found in nearly any volcanic edifice in island arc systems where uplift during volcanism is followed by subsidence after volcanism has ceased (Taylor, 1992). Eocene volcanic rocks, comprising the forearc basement in the IBM arc system, show a highly depleted composition of the source (extremely low Ti and Nb), widespread boninites, and a poorly developed bimodal basalt-rhyolite association. Therefore, their geochemical features are different from those of the Shishkhid ophiolite.

7.3. Island-arc rifting

Extension in an oceanic arc system begins with rifting that subsequently evolves into sea floor spreading. Intra-arc, back-arc or fore-arc rift settings can be distinguished, yet all are initiated by intra-arc rifting (Taylor, 1992). Morphologically, the fore-arc and back-arc rifts show similar features such as half-grabens, filled with volcanic breccias, turbidites, and calcareous ooze (Taylor, 1992). In both cases, rifting is associated with significant subsidence. After having examined the Cenozoic evolution of fore-arc, back-arc, and intra-arc rifting in the well studied IBM and Tonga-Lau systems (Gill et al., 1992; Hawkins, 1994, 1995; Martinez and Taylor, 2002; Gribble et al., 1998) we found that volcanic rocks of the Izu-Bonin back-arc extensional zone show a striking similarity with the Shishkhid lithology.

7.4. Izu-Bonin back-arc extensional zone

In the Izu-Bonin system crustal extension encompasses a 100 km-wide zone of generally shallow bathymetry between the frontal chain of huge stratovolcanoes and the Shikoku oceanic basin. Most of this area

is known as the “back-arc knolls zone” (Hochstaedter et al., 1990, 2000, 2001; Taylor, 1992). Crustal extension began about 2.8 Ma ago and was accompanied by bimodal basalt-rhyolite volcanism. West of the active extensional zone, there are the Western Seamounts that formed prior to extension. The seamounts consist of andesite, basaltic andesite, and basalt. Similar seamounts occur in the western part of the back-arc knolls zone. In its eastern part there is a chain of enechelon Quaternary grabens, adjacent to an active arc. Magmatism in these grabens began 0.6 Ma ago and has produced a bimodal assemblage of pillow basalt and rhyolite-dacite breccia. The volcanic rocks in all zones demonstrate an enrichment in slab-derived LILE which decreases from the volcanic front to the Western Seamounts (Hochstaedter et al., 1990, 2001; Gill et al., 1992).

The “knolls zone”, especially its western part, is composed of rocks showing remarkable similarity with the Shishkhdid volcanic assemblage. The zone exhibits two igneous associations, namely a bimodal rhyolite-basalt suite and andesites. The first group is regarded as related to rifting, whereas the second one is interpreted as related to magmatism producing the Western Seamount chains, whose extension to the knolls zone is designated as Eastern Seamounts. The REE patterns of both suites are variable between N- and E-MORB and may be explained by different degrees of melting and/or mixing of incompatible element-enriched and depleted mantle sources. ϵ_{Nd} values vary from +6.7 to +9.2, indicating melting of a variably depleted upper mantle. The

remarkable lithological and geochemical/isotopic similarity between the Shishkhdid ophiolite volcanic rocks and those in the Izu-Bonin back-arc knolls zone suggests a similar tectonic setting.

7.5. Geodynamic model for the origin of the Shishkhdid ophiolite

We propose that the Shishkhdid ophiolite formed during the initial stages of back-arc rifting. We further suggest that extension and rifting of island-arc lithosphere were caused by upwelling of asthenospheric mantle in an extensional back arc region. In such a setting, the mantle source was overprinted with subduction-slab fluids and possibly melts, whereas some magmas originated from fresh upwelling asthenosphere after stretching and thinning of the subduction-modified upper mantle (Fig. 14). Both magma types filled the extensional gaps in the arc crust and formed magma chambers with sheeted dykes in their roof. We do not know whether extension ever reached the sea-floor spreading stage, since we studied only a small fragment (in fact, a single “knoll”) of the island-arc system. Continued extension caused the studied Shishkhdid ophiolite to move away from the active volcanic zone. Magmatism continued for some time to the west of the ophiolite which implies that the frontal part of the Shishkhdid arc was facing westwards (in modern coordinates), whereas its eastern rear part, including the ophiolite section, was facing the back-arc oceanic basin. The other margin of the oceanic basin

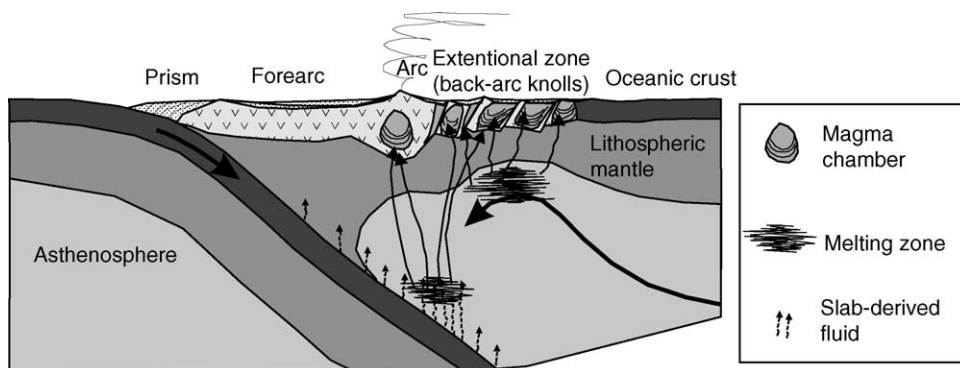


Fig. 14. Tectonic model proposed for the Shishkhdid ophiolite in analogy to the Recent Izu-Bonin back-arc knolls zone. Note location of magma sources in the subduction-modified mantle wedge and upwelling asthenosphere in the back of the rifted island arc. Modified after Gribble et al. (1998), Fig. 15 and Hochstaedter et al. (2001).

was formed by the Sarkhoi active continental margin with the adjacent Oka accretionary prism.

8. The Shishkhdid ophiolite belt

The thrust underlying the Shishkhdid ophiolite is a distinct suture demarcating two terranes that were separated by an oceanic basin in the late Neoproterozoic. The suture becomes obscured to the NE and SW of the Shishkhdid area due to metamorphism and deformation. Its presumed SW continuation is marked by a chain of serpentinite bodies and associated basalts trending through eastern and central Sangilen in the Tuva Autonomous Republic (Fig. 3). These ophiolite fragments are poorly studied, and the geochemistry of the volcanic rocks is unknown. A.V. Ilyin mapped the area at a scale of 1:200000 in the 1950s for the USSR Geological Survey and suggested that the serpentinites mark a major tectonic boundary because the lithologies to the north and south of it differ in composition (Ilyin, 2003, oral communication). However, the descriptions of these lithologies (Gibsher and Terleev, 1989, 1992) do not permit confident correlations with the Shishkhdid or Oka terrains.

It is conceivable that the suture extends into western Sangilen (Fig. 3) where detrital zircons from paragneisses yielded ages of 900–660 Ma (Salnikova et al., 2001; Kozakov et al., 2005). As the 2σ errors on these ages are large, these ages may be similar or younger than that of the Shishkhdid ophiolite. We therefore suggest West Sangilen to be a part of the Shishkhdid oceanic-arc terrain.

North of the Shishkhdid ophiolite, abundant minor serpentinite bodies enclosed in strongly metamorphosed rocks were reported. They are scattered over a considerable area and do not form a single linear zone (Nikitchin et al., 1983). To the NE the continuation of the Shishkhdid ophiolite belt is manifested by a chain of fragmented ophiolites along the northern limb of the Tuva-Mongolia Massif (Fig. 3). These rocks are mostly composed of serpentinite, but several major bodies also contain gabbro, basalt, and minor felsic intrusions (Sekerin et al., 1998, 2001). Diabase and basalt are characterized by low contents of TiO_2 , FeO, and K_2O , and exhibit calc-alkaline affinities. Similar to the Shishkhdid ophiolite, these bodies form the margin of the Oka accretionary prism. They probably belonged

to the Shishkhdid island-arc system in late Neoproterozoic times.

9. The Shishkhdid ophiolite and late Neoproterozoic tectonics of the Sayan-Balkalian region

9.1. Late Neoproterozoic palaeogeography

Three main tectonic zones of the Tuva-Mongolian Massif were delineated in Chapter 2, and three palaeogeographic features corresponded to them in the late Neoproterozoic. These are the Sarkhoi continental arc, Oka accretionary prism, and Shishkhdid oceanic arc (Fig. 15). The Sarkhoi volcanism set in after the early Baikalian orogeny at ~ 800 Ma with onset of subduction beneath the continental block. In the beginning, the active continental margin presumably belonged to the Siberian craton (Kuzmichev et al., 2001). Subsequently, a marginal block separated from the craton and formed the Japan-type Sarkhoi continental arc, fringed by the evolving Oka accretionary prism (Kuzmichev, 2004). The Shishkhdid arc constituted a separate island-arc system on the opposite side of the oceanic basin (Fig. 15a). Oceanic crustal fragments of this basin are tectonically intercalated within the Oka accretionary prism and are chiefly composed of MORB-type metabasalts (Sklyarov et al., 1996), associated with pelagic red shales and jaspers along the northern limb of the Oka belt (Kuzmichev, 2004).

9.2. Death of the Shishkhdid arc and birth of a new generation of island arcs

After the lithosphere of the oceanic basin which divided the Sarkhoi and Shishkhdid terranes had been completely subducted, the terranes collided, and the upper lithosphere of the rear part of the Shishkhdid arc was thrust upon the Oka accretionary prism. Collision-related granitoids in the Tuva-Mongolian Massif have not yet been found and, therefore, the age of collision has been inferred from geological evidence. An Ediacaran (late Vendian) to middle Cambrian carbonate platform sequence covers most of the Tuva-Mongolian Massif, and its basal horizons are composed of red clastic sediments filling the graben structures (Kuzmichev, 2004). The lowermost carbonate rocks are of late Ven-

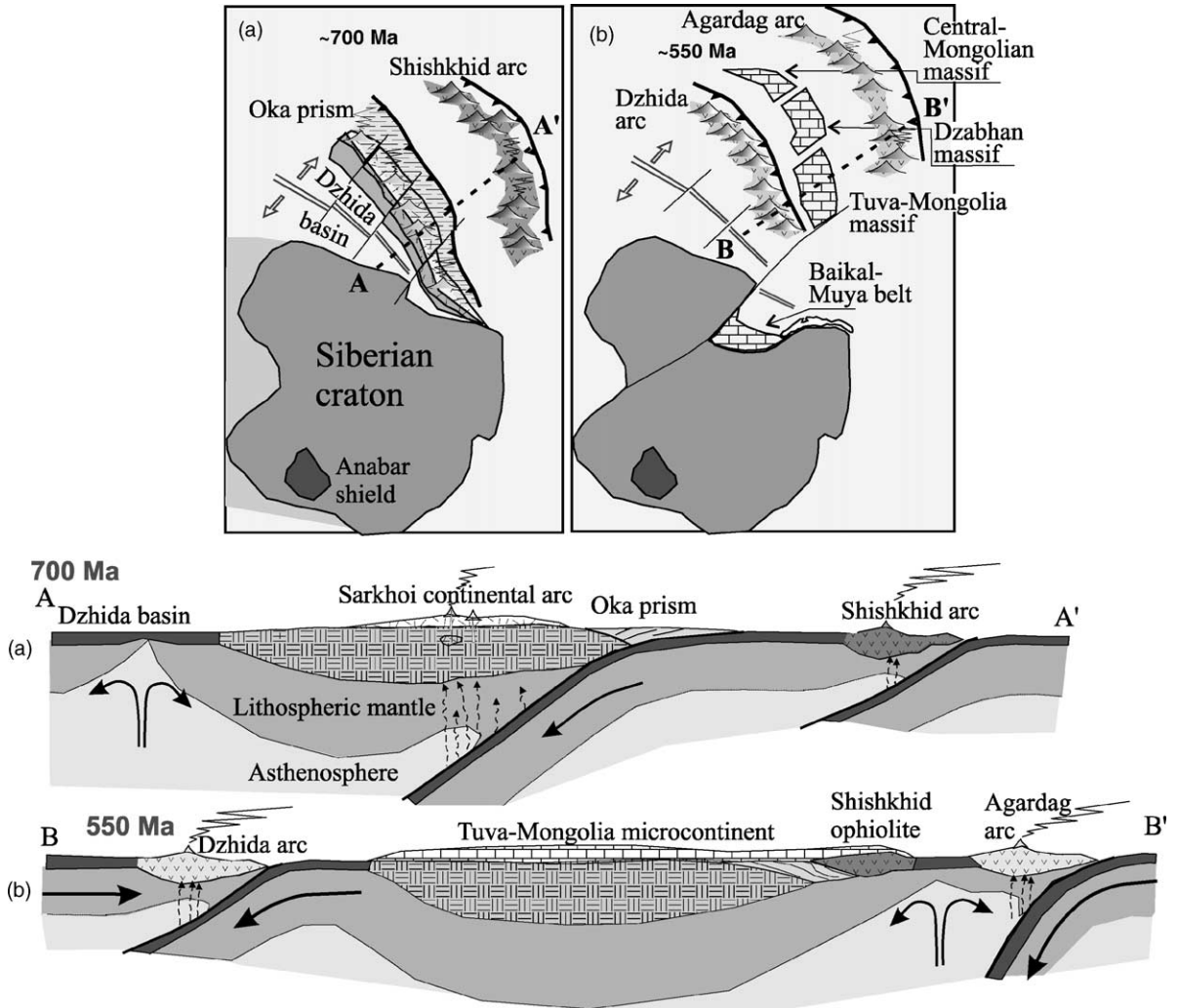


Fig. 15. Model for reconstruction of late Neoproterozoic to early Palaeozoic tectonics. (a) Relative position of the Shishkhid oceanic and Sarkhoi continental arcs at ~ 700 Ma (compare with Fig. 3). (b) Tuva-Mongolian microcontinent and other Precambrian terranes after the collision of the Shishkhid and Sarkhoi arcs and opening of Agardag back-arc oceanic basin as a result of late orogenic extension.

dian age (Terleev et al., 1998). The Shishkhid/Sarkhoi collision is conventionally placed at the early-late Vendian boundary, somewhere between 630 and 565 Ma (Bowring and Erwin, 1998; Khomentovsky, 2000, and references therein). We suggest an age of ~ 600 Ma for the collisional event and associate it with the late Baikalian orogenic phase which is widely manifested in southern Siberia (Khain and Rudakov, 1995; Rytsh et al., 2001; Kuzmichev, 2004).

After the Shishkhid arc was accreted to the Sarkhoi continental terrane, the Tuva-Mongolian microconti-

nent evolved in the form of carbonate platform fringed by a passive margin. The origin of the passive margin at the Shishkhid side of the microcontinent needs to be explained. Before being accreted, the Shishkhid arc was fringed by a convergent boundary from the outer oceanic side (Fig. 15a). The question is why subduction beneath the Shishkhid arc ceased after collision although plate convergence did not ends. An analogue may be a scenario similar to that currently operating in northern Taiwan (Teng, 1996). During the initial collisional phase, magmatism on the newly-formed active

continental margin continued for a short time of ca. 1 Ma. The evolving orogen subsequently collapsed and was rifted. The rift gave rise to the Okinawa back-arc trough as the Ryukyu arc moved away from the continent (Teng, 1996).

This tectonic development is compatible with the geology of the western Tuva-Mongolian Massif. In West Sangilen (Fig. 3), the Vendian to early Cambrian sediments display a facies change interpreted as a transition from a rifted passive continental margin to a back-arc basin and further to the Agardag island arc (Fig. 15b, profile; Gonikberg, 1997). This scenario also explains Vendian-Cambrian magmatism in the western Tuva-Mongolian Massif during accumulation of the carbonate platform deposits. The latter contain occasional dacites at the base of the section that correspond to the pre-rift phase. Tholeiitic basalt lavas or sills in the platform's higher horizons document the rift stage (Kuzmichev, 1991).

9.3. Analogues of Shishkhid ophiolite and manifestation of late Baikalian orogeny in other Precambrian terranes of southern Siberia

A Vendian-Cambrian platform cover, unconformably overlying Neoproterozoic complexes, is widespread in all Precambrian terrains of southern Siberia and western Mongolia. It provides evidence for the late Baikalian orogeny which resulted from widespread collision of late Neoproterozoic island arcs with a continental block. This is particularly true for the Dzabkhan (Zavkhan) Massif and the Baikal-Muya belt (Fig. 1), whose Neoproterozoic tectonic evolution resembles that of the Tuva-Mongolian Massif (Kuzmichev et al., 2001).

The Shishkhid ophiolite was previously interpreted as an equivalent of the Dariv (Daribie) ophiolite in the Dzabkhan Massif (Konnikov et al., 1994; Khain et al., 1995; Gibsher et al., 2001). These authors recognized a continuous "Daribie-Shishkhid zone". However, a zircon age of 571 ± 4 Ma for a plagiogranite of the Dariv ophiolite (Khain et al., 2003) disproves such a correlation and shows that this ophiolite is part of the late Vendian to early Cambrian Agardag–Tes–Chem island arc system which emerged after the Shishkhid arc had collided with the Sarkhoi continental terrane. However, at least two ophiolite assemblages of different age were recognized in the Dzabkhan massif (O. Tomurtoogoo,

personal communication, 2001). We suggest that one of these may be an extension of the Shishkhid belt.

The Baikal-Muya belt exhibits pervasive late Baikalian orogenic activity as documented by metamorphism up to amphibolite-facies (Konnikov et al., 1999) and emplacement of granitoids (Rytsk et al., 2001). A concordant zircon ages of 602 Ma for a tonalite and 590 Ma for a liparite were determined by E. Rytsk (2002, personal communication), whereas a calc-alkaline granite yielded a zircon age of 556 ± 16 Ma (Sryvtsev et al., 1992). Its pebbles were found in the lower horizons of the platform cover directly underlying carbonate rocks with an early Cambrian fauna (Rytsk et al., 2001). It is not clear what particular tectonic events triggered the late Baikalian orogeny in the Baikal-Muya belt. However, several Neoproterozoic island-arc and back-arc ophiolites were evidently involved in this event, yet their age is still controversial (Konnikov et al., 1999; Rytsk et al., 2001; Perelyaev, 2002).

Thus, the available information on the Dzabkhan Massif and Baikal-Muya belt is incomplete and controversial. Nevertheless it suggests that the late Neoproterozoic Shishkhid island-arc system originally had a considerable extension and was a major tectonic element of the Palaeo-Asian ocean.

10. Conclusions

The Shishkhid ophiolite represents a well-preserved ~13 km-thick section of uppermost oceanic lithosphere, comprising depleted mantle tectonites; gabbroic lower crust; sheeted dykes; a bimodal assemblage of basalt and rhyolite; and andesitic pyroclastic rocks on the top. The volcanic rocks are overlain by a 3 km-thick sedimentary sequence showing progressive subsidence of the volcanic edifice after cessation of volcanism. The crustal section of ophiolite was formed during arc rifting. The emerging gaps were filled with basaltic magma.

Most of the Shishkhid igneous rocks show a calc-alkaline fractionation trend, high abundances of LILE, as well as depletion of Nb relative to Th and LREE. These features indicate magma generation from a mantle source modified by fluids from a subducting slab. The variation in initial Nd isotopes ($\epsilon_{Nd} = +6.9$ to 0.0) can be explained by overprinting of a depleted sub-arc

mantle wedge source with a subducted sediment component. In addition, Th/Nb and LREE/Nb ratios show that some Shishkhid volcanic rocks originated from mantle sources that were not drastically affected by slab-derived components. ϵ_{Nd} values in this rock group range from +6.9 to +3.2 and probably indicate melting of upwelling heterogeneous asthenospheric sources in an evolving back-arc basin.

The composition of the Shishkhid volcanic rocks is amazingly similar to that in the “back-arc knolls zone” of the Izu-Bonin arc, and we suggest that the Shishkhid ophiolite formed in a similar setting.

SHRIMP U-Pb zircon dating of a rhyolite from the bimodal volcanic unit yielded a crystallization age of 800 ± 2.6 Ma. We assume that the Shishkhid arc began to form at this time and evolved throughout most of the late Neoproterozoic. Its evolution ended through collision with the Sarkhoi continental arc during the late Baikalian orogeny (~600 Ma).

Having identified the formation of late Neoproterozoic island arcs enables us to suggest a more refined model for the Neoproterozoic to early Palaeozoic tectonic evolution of the southern Siberian-Mongolian segment of the Central Asian fold belt. The new model includes three successive events of birth and death of island arc systems. These are: (1) latest Mesoproterozoic to early Neoproterozoic Dunzhugur arc (~1020–800 Ma, [Khain et al., 2002](#); [Kuzmichev et al., 2001](#)), (2) mid- to late Neoproterozoic Shishkhid arc (~800–600 Ma, this paper), and (3) formation of the late Vendian to early Cambrian Agardag–Tes–Chem–Dariv–Bayanhongor–Dzhida arc system (~570–500 Ma, [Khain et al., 2003](#); [Pfähnder et al., 2002](#); [Salnikova et al., 2001](#); [Badarch et al., 2002](#); [Pfähnder and Kröner, 2004](#)).

Acknowledgements

We thank Peter Cawood and Robert Stern for constructive reviews of the manuscript. The first author is grateful to his field assistants M.A. Svyatlovskaya (1988), E.E. Chernov (1989–1990), and to A.B. Dergunov—former chief of the Soviet-Mongolian expedition, who invited him to participate in fieldwork in Mongolia. A.K. thanks the German Academic Exchange Service (DAAD) for travel funding to visit the SHRIMP Laboratory in Beijing.

References

- Arculus, R.J., Pearce, J.A., Murton, B.J., van der Laan, S.R., 1992. Igneous stratigraphy and major-element geochemistry of holes 786a and 786b. In: Fryer, P., Pearce, J.A., Stokking, L.B. (Eds.), *Proceedings ODP, Scientific Results*, vol. 125, pp. 143–163.
- Badarch, G., Cunningham, W.D., Windley, B.F., 2002. A new terrane subdivision for Mongolia: implications for the Phanerozoic crustal growth of Central Asia. *J. Asian Earth Sci.* 21, 87–110.
- Bloomer, S.H., Taylor, B., MacLeod, C.J., Ctern, R.J., Frier, P., Hawkins, J.W., Johnson, L., 1995. Early arc volcanism and the ophiolite problem: a perspective from drilling in the western Pacific. In: Taylor, B., Natland, J. (Eds.), *Active margins and marginal basins of the western Pacific*. Am. Geophys. Union, *Geophysical Monograph*, vol. 88, pp. 1–30.
- Bowring, S.A., Erwin, D.H., 1998. A new look at evolutionary rates in deep time: uniting paleontology and high-precision geochronology. *GSA Today* 8, 1–7.
- Compston, W., Williams, I.S., Kirschvink, J.L., Zhang, Z., Ma, G., 1992. Zircon U–Pb ages for the early Cambrian time scale. *J. Geol. Soc. Lond.* 149, 171–184.
- Cousinaeu, P., 1994. A subaqueous pyroclastic deposits in an Ordovician fore-arc basin: an example from the Saint-Victor Formation, Quebec Appalachians. *Can. J. Sed. Res.* A64, 867–880.
- Defant, M.J., Drummond, M.S., 1990. Derivation of some modern arc magmas by melting of young subducted lithosphere. *Nature* 347, 662–665.
- Drummond, M.S., Defant, M.J., Kepezhinskas, P.K., 1996. Petrogenesis of slab-derived trondhjemite-tonalite-dacite/adakite magmas. *Trans. R. Soc. Edinburg: Earth Sci.* 87, 205–215.
- Garbe-Schonberg, C.-D., 1993. Simultaneous determination of thirty-seven trace elements in twenty-eight international rock standards by ICP-MS. *Geostand. Newslett.* 17, 81–97.
- Gibsher, A.S., Khain, E.V., Kotov, A.B., Sal'nikova, E.B., Kozakov, I.K., Kovach, V.P., Yakovleva, S.Z., Fedosenko, A.M., 2001. Late Vendian age of the Khan-Taishiri ophiolite complex in western Mongolia. *Geol. Geophys.* 42, 1179–1185.
- Gibsher, A.S., Terleev, A.A., 1989. The late Precambrian and early Palaeozoic regional stratigraphy of Sangilen. In: Khomevovskiy, V. (Ed.), *Late Precambrian and Early Palaeozoic Structural Complexes of Sangilen and South-Eastern Tuva*. Institute of Geology and Geophysics, Russian Academy of Sciences, Novosibirsk, pp. 3–26 (in Russian).
- Gibsher, A.S., Terleev, A.A., 1992. The stratigraphy of the Upper Precambrian and Lower Cambrian in south-east Tuva and North Mongolia. *Geol. Geophys.* 33, 26–35.
- Gill, J.B., Seales, C., Thompson, P., Hochstaedter, A.G., Dunlap, C., 1992. Petrology and geochemistry of Pliocene-Pleistocene volcanic rocks from the Izu arc Leg 126. In: Taylor, B., Fujioka, K. (Eds.), *Proceedings ODP, Scientific Results*, vol. 126, pp. 383–404.
- Gonikberg, V.E., 1997. Paleotectonic nature of northwestern margin of the Sangilen Massif (Tuva) in the late Precambrian. *Geotectonics* 31, 408–419.
- Gribble, R.F., Stern, R.J., Newman, S., Bloomer, S.H., O'Hearn, T., 1998. Chemical and isotopic composition of lavas from the

- northern Mariana Trough: implications for magma genesis in back-arc basins. *J. Petrol.* 39, 125–154.
- Hanchar, J.M., Miller, C.F., 1993. Zircon zonation patterns as revealed by cathodoluminescence and backscattered electron images: implications for interpretation of complex crustal histories. *Chem. Geol.* 110, 1–13.
- Hawkins, J.W., 1994. Petrologic synthesis: the Lau Basin transect. In: Hawkins, J., Parson, L., Allan, J. (Eds.), *Proceedings ODP, Scientific Results*, vol. 135, pp. 879–908.
- Hawkins, J.W., 1995. Evolution of the Lau Basin- Insights from ODP Leg 135. In: Taylor, B., Natland, J. (Eds.), *Active margins and marginal basins in the western Pacific*. *Am. Geophys. Union, Geophys. Monogr.* 88, 125–173.
- Hegner, E., Walter, H.J., Satir, M., 1995. Pb–Sr–Nd isotopic compositions and trace element geochemistry of megacrysts and melilitites from the Tertiary Urach volcanic field: source composition of small volume melts under SW Germany. *Contrib. Mineral. Petrol.* 122, 322–335.
- Hochstaedter, A.G., Gill, J.B., Morris, J.D., 1990. Volcanism in the Sumisu rift. II. Subduction and non-subduction related component. *Earth Planet. Sci. Lett.* 100, 195–209.
- Hochstaedter, A.G., Gill, J.B., Taylor, B., Ishizuka, O., Yuasa, M., Morita, S., 2000. Across arc geochemical trends in the Izu-Bonin arc: constraints on source composition and mantle melting. *J. Geophys. Res.* 105, 495–512.
- Hochstaedter A., Gill J., Peters R., Broughton P., Holden P., 2001. Across arc geochemical trends in the Izu-Bonin arc: contributions from the subduction slab. *Geochem. Geophys. Geosyst.*, 2, 44, paper number 2000GC000105.
- Ilyin, A.V., 1971. On the Tuva-Mongolia massif. In: *Materials on Regional Geology of Africa and Foreign Asia*. *Transactions of NIIZarubezhgeologia* (22) 67–73 (in Russian).
- Ilyin, A.V., 1982. Geologic evolution of South Siberia and Mongolia in late Precambrian and Cambrian. *Nauka Publ. House, Moscow*, 114 pp. (in Russian).
- Isakov, V.M., Korobeinikov, V.P., Abramov, A.V., 1981. Precambrian stratigraphy of western part of the East Tuva orogenic trough Actual problems of Precambrian geology of Siberia. *Proc. Siberian Institute of Geology, Geophysics and Mineral Deposits*, vol. 290, 36–42 (in Russian).
- Jacobsen, S.B., Wasserburg, G.J., 1980. Sm–Nd isotopic evolution in chondrites. *Earth Planet. Sci. Lett.* 50, 139–155.
- Kennedy, A.K., De Laeter, J.R., 1994. The performance characteristics of the WA SHRIMP II ion microprobe. *U.S. Geol. Surv. Circular* 1107, 166.
- Khain, E.V., Amelin, Yu.V., Izokh, A.E., 1995. Sm–Nd data on the age of ultrabasic-basite complexes in the obduction zone, western Mongolia. *Trans. (Doklady) Russ. Acad. Sci., Earth Sci.* 341, 791–796 (in Russian).
- Khain, E.V., Bibikova, E.V., Kröner, A., Zhuravlev, D.Z., Sklyarov, E.V., Fedotova, A.A., Kravchenko-Berezhnoy, I.R., 2002. The most ancient ophiolite of the central Asian fold belt: U–Pb and Pb–Pb zircon ages for the Dunzhugur Complex, Eastern Sayan, Siberia, and geodynamic implications. *Earth Planet. Sci. Lett.* 202, 1–16.
- Khain, E.V., Bibikova, E.V., Salmnikova, E.B., Kröner, A., Gibsher, A.S., Didenko, A.N., Degtyarev, K.E., Fedotova, A.A., 2003. The Palaeo-Asian ocean in the Neoproterozoic and early Palaeozoic: new geochronologic data and palaeotectonic reconstructions. *Precambrian Res.* 122, 329–358.
- Khain, V.E., Rudakov, S.G., 1995. The Baikalian orogeny after N.S.Shatsky and the Baikalian epoch of tectogenesis. *Stratigr. Geol. Correl.* 3, 2–32.
- Khomentovskiy, V.V., 2000. Substantiation of the Vendian-Lower Cambrian geochronological scale by U–Pb zircon ages. *Baikalian in Siberia*. *Russ. Geol. Geophys.* 41, 503–515.
- Kinny, P.D., 1986. 3820 Ma zircons from a tonalitic Amitsoq gneiss in the Godthab district of southern West Greenland. *Earth Planet. Sci. Lett.* 79, 337–347.
- Konnikov, E.G., Gibsher, A.S., Izokh, A.E., Sklyarov, E.V., Khain, E.V., 1994. Late-Proterozoic evolution of northern segment of the Palaeoasian Ocean: new radiological and geochemical data. *Russ. Geol. Geophys.* 35, 152–168.
- Konnikov, E.G., Tsygankov, A.A., Vrublevskaia, T.T., 1999. The Baikal-Muya Volcanic and Plutonic Belt: Structure, Substance and Geodynamics. *GEOS Publ. House, Moscow*, 163 pp.
- Kozakov, I.K., Sal'nikova, E.B., Nutman, A., Kovach, V.P., Kotov, A.B., Podkovyrov, V.N., Plotkina, U.V., 2005. Metaterrigenous metamorphic rocks in Tuva-Mongolian Massif: age, sources and tectonic setting. *Stratigr. Geol. Correl.* 13, 1–20.
- Kuzmichev, A.B., 1991. Geology and stratigraphy of Bilin subzone of the Shishkhid ophiolite belt (Eastern Tuva and northern Mongolia). In: Khomentovskiy, V.V. (Ed.), *Late Precambrian and early Paleozoic of Siberia. Siberian Platform and its Fringing*. *Russian Academy of Sciences, Siberian Branch, Novosibirsk, Institute of Geology and Geophysics*, pp. 130–150 (in Russian).
- Kuzmichev, A.B., 2004. Tectonic History of the Tuva-Mongolian Massif: Early Baikalian, Late Baikalian and Early Caledonian Stage. *Probl. Moscow*, 192 pp. (in Russian).
- Kuzmichev, A.B., Bibikova, E.V., Zhuravlev, D.Z., 2001. Neoproterozoic (~800 Ma) orogeny in the Tuva–Mongolia Massif (Siberia): Island arc–continent collision at the northeast Rodinia margin. *Precambrian Res.* 110, 109–126.
- Kuzmichev, A.B., Zhuravlev, D.Z., 1999. Pre-Vendian age of the Oka Group, eastern Sayany: Evidence from Sm–Nd dating of sills. *Trans. (Doklady) Russ. Acad. Sci., Earth Sci. Section* 365, 173–178.
- Lagabrielle, Y., Sizun, J.-P., Arculus, R.J., 1992. The constructional and deformational history of the igneous basement penetrated at site 786. In: Fryer, P., Pearce, J.A., Stokking, L.B. (Eds.), *Proceedings ODP, Scientific Results*, vol. 125, pp. 263–276.
- Leitch, E.C., 1984. Marginal basins of the SW Pacific and the preservation and recognition of their ancient analogues: a review. In: Kokelaar, B.P., Howells, M.F. (Eds.), *Marginal Basin Geology*, 16. *Special Publ. Geol. Society London*, pp. 97–108.
- Lesnov, F.P., Melyakhovskiy, A.A., Bayarkhuu, Zh., 1977. The Shishkhid ultramafic massif (northern Mongolia). In: *Materials on genetic mineralogy and petrology*. *Institute of Geology and Geophysics, Russian Academy of Sciences, Novosibirsk*, pp. 130–145 (in Russian).
- Martinez, F., Taylor, B., 2002. Mantle wedge control on back-arc crustal accretion. *Nature* 416, 417–420.

- McCulloch, M.T., Gamble, J.A., 1991. Geochemical and geodynamical constraints on subduction magmatism. *Earth Planet. Sci. Lett.* 102, 358–374.
- Melaykhovetsky, A.A., 1982. Metamorphism of the eastern Tuva ultramafics. Nauka Publ. House, Novosibirsk, 134 pp. (in Russian).
- Melaykhovetsky, A.A., Lesnov, F.P., 1976. On the ultramafics of the Shishkhidgol massif (Mongolia). *Russ. Geol. Geophys.* 17, 144–149 (in Russian).
- Nelson, D.R., 1997. Compilation of SHRIM U–Pb zircon geochronology data. 1996 Geol. Surv. Western Australia, Record, 1997/2, 189 pp.
- Nikitchin, P.A., Shibanov, V.I., Bukharov, N.S., Chuchko, V.N., Aleksandrov, G.P., 1983. Geological map of Tuva. In: Podkamennyi, A.A., Sherman, M.L., Nikitchin, P.A., Shaposhnikov, G.N. (Eds.), Geological map of Tuva, scale 1:500 000. All-Russian Geological Research Institute, St. Petersburg (in Russian).
- Pearce, J.A., van der Laan, S., Arculus, R.J., Murton, B.J., Ishii, T., Peate, D.W., Parkinson, I.J., 1992. Boninite and harzburgite from Leg 125 (Bonin-Mariana forearc): a case study of magma genesis during the initial stages of subduction. In: Frier, P., Pearce, J.A., Stoking, L.B. (Eds.), Proceedings ODP, Scientific Results, vol. 125, pp. 623–659.
- Perelyaev, V.I., 2002. Ultramafic and mafic complexes of western Middle-Vitim highland. Unpubl. summary of candidate thesis. Institute of the Earth Crust, Russian Academy of Sciences Irkutsk, 18 pp. (in Russian).
- Pfänder, J.A., Jochum, K.P., Kozakov, I., Kröner, A., Todt, W., 2002. Coupled evolution of back-arc and island arc-like mafic crust in the late Neoproterozoic Agardagh Tes-Chem ophiolite, central Asia: evidence from trace element and Sr–Nd–Pb isotope data. *Contrib. Mineral. Petrol.* 143, 154–174.
- Pfänder, J.A., Kröner, A., 2004. Tectono-magmatic evolution, age and emplacement of the Agardagh Tes-Chem ophiolite in Tuva, Central Asia: Crustal growth by island arc accretion. In: T. Kusky (Ed.), *Precambrian ophiolites and related rocks*. Elsevier, Amsterdam, pp. 207–221.
- Pidgeon, R.T., Macambira, M.J.B., Lafon, J.M., 2000. Th–U–Pb isotopic systems and internal structures of complex zircons from an enderbite from the Pium Complex, Carajas Province, Brazil: evidence for the ages of granulite facies metamorphism and the protolith of the enderbite. *Chem. Geol.* 166, 159–171.
- Rytsk, E.Yu., Amelin, Yu.V., Rizvanova, N.G., Krymskii, R.Sh., Mitrofanov, G.L., Mitrofanova, N.N., Perelyaev, V.I., Shalaev, V.S., 2001. Age of rocks in the Baikal-Muya foldbelt. *Stratigr. Geol. Correl.* 9, 3–15.
- Salmikova, E.B., Kozakov, I.K., Kotov, A.B., Kröner, A., Todt, W., Nutman, A., Yakovleva, S.Z., Kovach, V.P., 2001. Age of Palaeozoic granites and metamorphism in the Tuva-Mongolia massif of the Central Asian Mobile Belt: loss of a Precambrian microcontinent. *Precambrian Res.* 110, 143–164.
- Sekerin, A.P., Men'shagin, Yu.V., Laschenov, V.A., Sekerina, N.V., 1998. On a new ophiolitic belt in eastern Sayan. *Bull. Moscow Soc. Natural.* 73, 12–15 (in Russian).
- Sekerin, A.P., Men'shagin, Yu.V., Yegorov, K.N., 2001. Yekheshignin ultramafic massif of the Belsk-Dugda ophiolite belt, eastern Sayan. *Domestic Geol.* 1, 45–51 (in Russian).
- Shervais, J.W., 2001. Birth, death and resurrection: the life cycle of suprasubduction zone ophiolites. *Geochem. Geophys. Geosyst.* 2, 45, paper number 2000GC000080.
- Sklyarov, E.V., Postnikov, A.A., Posokhov, V.F., 1996. Structural setting, metamorphism and petrology of Hügeyn group (northern Mongolia). *Russ. Geol. Geophys.* 37, 69–78.
- Sryvtsev, N.A., Khalilov, V.A., Buldygerov, V.V., Perelyaev, V.I., 1992. Geochronology of the Baikal-Muya belt granitoids. *Russ. Geol. Geophys.* 33, 15–24.
- Stern, R.J., Bloomer, S.H., 1992. Subduction zone infancy: examples from the Eocene Izu-Bonin-Mariana and Jurassic California arcs. *Geol. Soc. Am. Bull.* 104, 1621–1636.
- Stix, J., 1991. Subaqueous, intermediate to silicic-composition explosive volcanism: a review. *Earth Sci. Rev.* 31, 21–53.
- Sun, S.S., McDonough, W.F., 1989. Chemical and isotopic systematics of oceanic basalts: implications for mantle composition and processes. In: Saunders, A.D., Norry, M.J., (Eds.), *Magmatism in the ocean basins*, *Geol. Soc.* 42, 313–345 (special publication).
- Takagi, T., Orihashi, Y., Naito, K., Watanabe, Y., 1999. Petrology of a mantle-derived rhyolite, Hokkaido. *Jpn. Chem. Geol.* 160, 425–445.
- Tamura, Y., 1995. Liquid lines of descent of island arc magmas and genesis of rhyolites: evidence from the Shirahama group. *Jpn. J. Petrol.* 36, 417–434.
- Tamura, Y., Tatsumi, Y., 2002. Remelting of an andesitic crust as a possible origin for rhyolitic magma in oceanic arcs: an example from the Izu-Bonin arc. *J. Petrol.* 43, 1029–1047.
- Taylor, B., 1992. Rifting and the volcanic-tectonic evolution of the Izu-Bonin-Mariana arc. In: Taylor, B., Fujioka, K., et al. (Eds.), *Proceedings ODP, Scientific Results*, vol. 126, pp. 627–652.
- Teng, L.S., 1996. Extensional collapse of the northern Taiwan mountain belt. *Geology* 24, 949–952.
- Terleev, A.A., Postnikov, A.A., Karlova, G.A., Nagovitsyn, K.E., Sushakova, A.V., 1998. New data on the age of Zabit Formation in eastern Sayan (Vendian and early Cambrian). *Actual problems of geology and geography of Siberia*, 1. Tomsk University, pp. 312–314 (in Russian).
- Vavra, G., 1990. On the kinematics of zircon growth and its petrogenetic significance: a cathodoluminescence study. *Contrib. Mineral. Petrol.* 106, 90–99.
- Vavra, G., Gebauer, D., Schmidt, R., Compston, W., 1996. Multiple zircon growth and recrystallization during polyphase Late Carboniferous to Triassic metamorphism in granulites of the Ivrea Zone (southern Alps): an ion microprobe (SHRIMP) study. *Contrib. Mineral. Petrol.* 122, 337–358.